lubricants

MDPI

Article

The Effect of Dry Friction upon the Dynamics of a Short Eccentric Rotor: An Analytical and Experimental Study

Stelian Alaci [1,*], Ilie Musca [1], Carmen Bujoreanu [2], Ionut-Cristian Romanu [1], Nicolae-Adrian Nitu [2] and Florina-Carmen Ciornei [1]

[1] Mechanics and Technologies Department, Stefan cel Mare University of Suceava, 720229 Suceava, Romania; ilie.musca@usm.ro (I.M.); ionutromanucristian@usm.ro (I.-C.R.); florina.ciornei@usm.ro (F.-C.C.)
[2] Mechanical Engineering, Mechatronics and Robotics Department, "Gheorghe Asachi" Technical University, 700050 Iasi, Romania; carmen.bujoreanu@academic.tuiasi.ro (C.B.); nicolae-adrian.nitu@student.tuiasi.ro (N.-A.N.)
* Correspondence: stelian.alaci@usm.ro

Abstract: The paper proposes the study of dry friction by means of a short eccentric rotor. The rotor was designed and realised in the laboratory. In an ideal frictionless situation, a rotor actuated by gravity will have an angular velocity which increases indefinitely. The analytical model assumes dry friction in the bushing of the rotor and the main result reveals that the angular velocity either stabilizes around a certain value or drops to zero. Two situations of friction were considered for the theoretical model: first only dynamic friction and secondly, both static and dynamic friction are present. The analytical model of the dynamics of the rotor presents the advantage that it can be applied for diverse friction cases, from dry friction to complex dry friction and wet friction. Experimental tests were carried out on the designed and constructed device; they are in very good agreement with the results of the theoretical model.

Keywords: dry friction; static coefficient of friction; dynamic coefficient of friction; nonlinear dynamical system; short eccentric rotor

Citation: Alaci, S.; Musca, I.; Bujoreanu, C.; Romanu, I.-C.; Nitu, N.-A.; Ciornei, F.-C. The Effect of Dry Friction upon the Dynamics of a Short Eccentric Rotor: An Analytical and Experimental Study. *Lubricants* **2023**, *11*, 340. https://doi.org/10.3390/lubricants11080340

Received: 24 May 2023
Revised: 21 July 2023
Accepted: 7 August 2023
Published: 9 August 2023

1. Introduction

There are few situations in modern engineering applications where a solid part fulfils a unique certain task independently. In most cases the body interacts with other bodies by direct contact or by means of a field (magnetic, electric etc.). For the contacting bodies, they share points, segments of curves or surfaces and thus they form kinematic pairs. Before contacting, each part of the pair has a number of degrees of freedom but after the contact is made, the kinematic effect resides in the diminution of the degrees of freedom of one of the parts.

A first classification criterion of kinematic pairs consists in the number of degrees of freedom (DOF) removed by the pair. For the pairs, the lower the class, the greater the difficulty of controlling the relative motion between the two elements. Thus, the conclusion is reached that, from the point of view of motion control from a kinematic pair, the most desirable are of the fifth-class pairs, revolute or translational, where the relative position between the elements of the pair is described by a single scalar parameter. An adequate example in this case can be a robotic structure [1], where, for ensuring the DOF for the final element, a kinematic chain is used, having in the structure driving kinematic pairs of fifth class. Another notable illustration, frequently met in engineering, is the kinematic revolute pair. It consists in an immobile element (stator) and a mobile element (rotor) that rotates about an axis. The dynamical behaviour of rotors was profoundly studied [2–7] but it remains an actual topic [8–10]. Numerous aspects must be considered in analysing the running of a rotor, such as the ratio between the length of the rotor and the dimension of the cross section; in addition, there are the long rotors, whose axial dimension is much greater

than their cross-sectional dimension [11,12] and the short rotors [13,14], having this ratio less than 1 (proper fraction). Another extremely important aspect is the manner in which the rotor is supported [15–17]; more precisely, the type of employed bearing (plain bearing or roller bearing). In the case of the plain bearing, the type of friction, dry or fluid, is a significant parameter. Most plain bearings work under fluid lubrication conditions [18–20], but there are situations when the functioning conditions impose the use of dry friction bushings [10,21]. Another characteristic to be discussed concerns rotor balancing. The balancing operation is mandatory because the magnitude of unbalance defines the inertial forces acting upon the rotor and the reactions from the bearings [22,23].

Another aspect of critical importance refers to the vibrations of the rotor. A first cause producing vibrations is the supporting modality, where for deformable parts of the bearing the vibration occurrence is inevitable. In the case of long rotors, assuming the hypothesis of deformable body, the rotor will have infinite vibration modes [24,25]. For an unbalanced rotor, the inertia forces that have a radial direction will act as exciting forces and may produce the resonance phenomenon; when the deformations increase over the admissible limit, cracks occur and finally the entire system deteriorates.

The briefly above-mentioned considerations permit the conclusion that the dynamic study of a rotor is a difficult task [26,27] if all the parameters mentioned are to be included; therefore, in the literature there are simpler or more complex dynamical models [28], according to the accepted simplifying hypotheses [29–32].

In recent years, many scientific papers have been published that present new methods of studying rotors [33–35]. The dynamic and resonance response of rotational shafts having different types of blades was analysed and presented by [36,37]. The nonlinear behaviour imposes the necessity of developing advanced numerical models and considering nonlinearity [38,39].

The authors consider that the main justification of this paper consists in presenting a model for a simple dynamic system, a short rotor actuated by gravity, whose equation of motion is strongly nonlinear. Two causes are the basis of nonlinearity: the presence of dry friction in the bearing of the rotor and the existence of two characteristic solutions of the motion of the system, from which only one corresponds to physical reality, the other one being induced by solving an irrational equation. We had two main objectives in the paper: to explore the effect of the adopted model of dry friction upon the evolution of the theoretical system and the experimental validation of the theoretical model. The adopted friction models are two of the simplest from the literature: first, the model where the friction force is characterised by the coefficient of dynamic friction and second, the model where while the relative velocity decreases under a certain critical value the friction force is accepted to be described using the coefficient of static friction and beyond this value, the friction presents a dynamic character. A test rig from the laboratory was used to evidence that the first model of dynamic friction describes much better the actual behaviour of the system.

Most of the studies about rotor dynamics consider deformable rotors, and one of the main objectives becomes finding the stress state occurring during running. Some of the works from the literature also study the concentrator effect caused by different material defects or by the shape.

There are also situations when the rigid rotor hypothesis is perfectly plausible, namely when the angular velocity of the rotor is much smaller than the critical angular velocity of the rotor. Such a situation is considered in the present work, where, for an experimental rotor, the proper frequency values were found, and it was established that the first one is much greater that the regime one. At first sight it could seem that the rigidity assumption simplifies substantially the study, but the present work shows the opposite. For the concrete situation of a short rotor actuated by gravity, by applying the general theorems of dynamics of rigid bodies, a system of differential equations results. The equations are strongly nonlinear and permit finding the law of motion of the rotor, the low of rotation of the normal reaction and its magnitude.

2. Materials and Methods

2.1. Long Rotor Dynamic Equations

The problem of the modelled rotor consists in finding the law of motion and the reactions from the kinematical joints. All components, the rotor and the stator (plain bearing) are considered rigid bodies.

A rotor consisting in two cylindrical regions is shown in Figure 1; it can rotate about an axis defined by the two cylindrical regions (1) and (2). The rotor is not balanced, because, as can be observed, the centre of mass denoted Γ is not positioned on the axis of rotation. A fixed coordinate system $OXYZ$ is considered that has the OZ axis in *coincidence* with the axis of rotation. Dynamic study requires a mobile coordinate system, attached to the rotor. This frame is chosen in order to have the axis Oz in coincidence with the axis of rotation OZ. The Ox axis of the mobile frame is normal to the axis of rotation and passes through the centre of mass Γ of the rotor, placed at the distance x_M from the axis of rotation. The Oy axis completes a triorthogonal right coordinate frame. The unique external force acting upon the rotor is the own weight $\boldsymbol{G}$. In the bearings where the cylindrical regions (1) and (2) take part, a contact pressure is developed which generates a system of normal elementary forces. Each distribution of normal forces can be equivalated to a normal reaction, denoted $\boldsymbol{N}_1$ and $\boldsymbol{N}_2$, respectively, acting in a plane P_1 and P_2, respectively, normal to the axis of rotation and passing through the points C_1 and C_2. The distribution of normal forces from the bearing will generate, in its turn, a distribution of elementary tangential forces opposing the relative motion between the points in contact that can be replaced by finite friction force, acting tangent to the surface of the bearing.

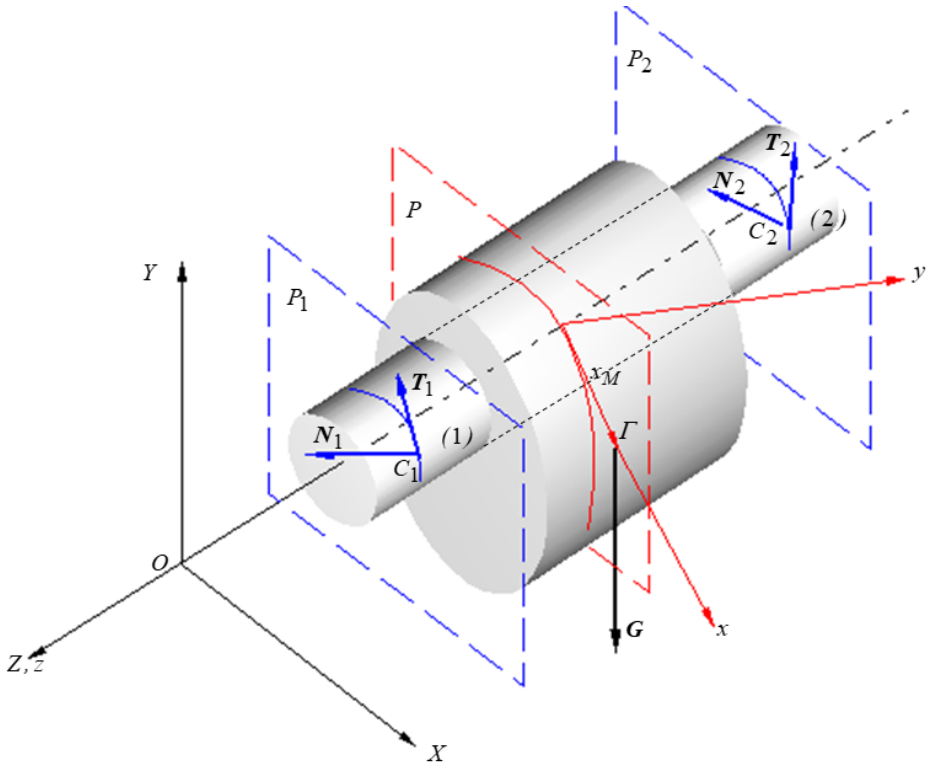

Figure 1. Schematics of a long rotor.

Therefore, two friction forces, $\boldsymbol{T}_1$ and $\boldsymbol{T}_2$ can be considered and, assuming that the bearing does not present axial displacements, then $\boldsymbol{T}_1$ and $\boldsymbol{T}_2$ will act in the points C_1 and C_2, respectively, and will be contained in the plane P_1 and P_2, respectively.

In order to solve the problem, two fundamental theorems are applied:

- the motion of the centre of mass theorem (a particular case of impulse–momentum theorem)

$$\dot{\boldsymbol{H}} = \boldsymbol{G} + \boldsymbol{N}_1 + \boldsymbol{N}_2 + \boldsymbol{T}_1 + \boldsymbol{T}_2 \tag{1}$$

where $\boldsymbol{H}$ is the impulse of the rotor.

- the angular momentum theorem with respect to the centre of mass Γ

$$\dot{\boldsymbol{K}}_\Gamma = \widetilde{\boldsymbol{r}}_{C_1}(\boldsymbol{N}_1 + \boldsymbol{T}_1) + \widetilde{\boldsymbol{r}}_{C_2}(\boldsymbol{N}_2 + \boldsymbol{T}_2) \tag{2}$$

where $\boldsymbol{K}_\Gamma$ is the angular momentum, $\widetilde{\boldsymbol{r}}_{C_1}, \widetilde{\boldsymbol{r}}_{C_2}$ are the anti-symmetric matrices associated to the vectors $\boldsymbol{r}_{C_1}, \boldsymbol{r}_{C_2}$.

Matrix Equations (1) and (2) are projected on the axes of the mobile system and a set of six scalar equations results. Due to the lack of axial motion, the projection of Equation (1) on Oz axis conducts to an identity and then, only five scalar equations are available. For the case of long bearing, the unknowns of the problem are the positional parameter of the rotor and the magnitudes and directions of the normal reactions N_1 and N_2. It is noteworthy that because the reactions belong to planes normal to the axis of rotation, the versors of the two normal can be defined using a single parameter.

$$\boldsymbol{u}_{N_{1,2}} = (cos\psi_{1,2}, sin\psi_{1,2}, 0) \tag{3}$$

The left member of relation (2) in explicit form is:

$$\dot{\boldsymbol{K}}_\Gamma = \begin{bmatrix} J_x & -J_{xy} & -J_{xz} \\ -J_{xy} & J_y & -J_{yz} \\ -J_{xz} & -J_{yz} & J_z \end{bmatrix} \begin{bmatrix} 0 \\ 0 \\ \ddot{\varphi} \end{bmatrix} + \begin{bmatrix} 0 & -\dot{\varphi} & 0 \\ \dot{\varphi} & 0 & 0 \\ 0 & 0 & 0 \end{bmatrix} \begin{bmatrix} J_x & -J_{xy} & -J_{xz} \\ -J_{xy} & J_y & -J_{yz} \\ -J_{xz} & -J_{yz} & J_z \end{bmatrix} \begin{bmatrix} 0 \\ 0 \\ \dot{\varphi} \end{bmatrix} = \begin{bmatrix} -J_{xz}\ddot{\varphi} + J_{yz}\dot{\varphi}^2 \\ -J_{yz}\ddot{\varphi} - J_{xz}\dot{\varphi}^2 \\ J_z\ddot{\varphi} \end{bmatrix} \tag{4}$$

and with the explicit right member of relation (2), it results:

$$\begin{aligned} \widetilde{\boldsymbol{r}}_{C_1}(\boldsymbol{N}_1 + \boldsymbol{T}_1) + \widetilde{\boldsymbol{r}}_{C_2}(\boldsymbol{N}_2 + \boldsymbol{T}_2) &= \widetilde{\boldsymbol{r}}_{C_1}(N_1\boldsymbol{u}_{N_1} + (\widetilde{\boldsymbol{k}}(T_1\boldsymbol{u}_{N_1}) + \widetilde{\boldsymbol{r}}_{C_2}(N_2\boldsymbol{u}_{N_2} + (\widetilde{\boldsymbol{k}}(T_2\boldsymbol{u}_{N_2}) \\ &= \begin{bmatrix} -z_{C_1}(N_1 sin\psi_1 + T_1 cos\psi_1) - z_{C_2}(N_2 sin\psi_2 + T_2 cos\psi_2) \\ z_{C_1}(N_1 cos\psi_1 - T_1 sin\psi_1) + z_{C_2}(N_2 cos\psi_2 - T_2 sin\psi_2) \\ (x_{C_1} sin\psi_1 - y_{C_1} cos\psi_1)N_1 + (x_{C_1} cos\psi_1 + y_{C_1} sin\psi_1)T_1 + \\ (x_{C_2} sin\psi_2 - y_{C_2} cos\psi_1)N_2 + (x_{C_2} cos\psi_2 + y_{C_2} sin\psi_1)T_2 \end{bmatrix} \end{aligned} \tag{5}$$

Closing, the equations of projection of the angular momentum theorem with respect to the centre of mass are:

$$\begin{cases} -J_{xz}\ddot{\varphi} + J_{yz}\dot{\varphi}^2 = -z_{C_1}\left(N_1 sin\psi_1 + T_1 cos\psi_1\right) - z_{C_2}(N_2 sin\psi_2 + T_2 cos\psi_2) \\ -J_{yz}\ddot{\varphi} - J_{xz}\dot{\varphi}^2 = z_{C_1}(N_1 cos\psi_1 - T_1 sin\psi_1) + z_{C_2}(N_2 cos\psi_2 - T_2 sin\psi_2) \\ J_z\ddot{\varphi} = \left(x_{C_1} sin\psi_1 - y_{C_1} cos\psi_1\right)N_1 + \left(x_{C_1} cos\psi_1 + y_{C_1} sin\psi_1\right)T_1 + \\ \left(x_{C_2} sin\psi_2 - y_{C_2} cos\psi_1\right)N_2 + \left(x_{C_2} cos\psi_2 + y_{C_2} sin\psi_2\right)T_2 \end{cases} \tag{6}$$

For the case of short rotor, the dimensions on the direction of the axis of rotation Oz are much smaller than the dimensions from the other two directions, are considered at limit equal to zero, and then the right members of the first two equations of system (6) also tend to zero.

From the definition of the inertia products J_{xz} and J_{yz}:

$$J_{xz} = \int_M xzdm,\ J_{yz} = \int_M yzdm \tag{7}$$

It is noticed that:

$$\lim_{z\to 0} J_{xz} = \lim_{z\to 0} J_{yz} = 0 \tag{8}$$

and therefore, for the short rotor, the first two equations become identities. In conclusion, for the short rotor case, the dynamics' theorems provide three scalar equations: two equations

are obtained by projecting the centre of mass theorem on the axes Ox and Oy and the third equation results from the projection of the angular momentum theorem on the direction of the rotation axis Oz. From here it results that, for the short rotor, the system of equations must have three unknowns. One of the unknowns—which also occurs in the case of long rotor—is φ, the angle of rotation of the rotor. The rotor has a single degree of freedom and from here it results that the other two scalar unknowns are required for characterisation of the reactions. From relation (1) it is suggested that the normal reaction $\boldsymbol{N}$ and the tangential reaction $\boldsymbol{T}$ can be introduced as unknowns.

$$\boldsymbol{N} = \boldsymbol{N}_1 + \boldsymbol{N}_2;\ \boldsymbol{T} = \boldsymbol{T}_1 + \boldsymbol{T}_2 \tag{9}$$

The introduction of the new variables must be compatible with the last equation of the system (6) and from the relation (2) it is observed that it is required that the normal reactions $\boldsymbol{N}_1, \boldsymbol{N}_2$ and tangential reactions $\boldsymbol{T}_1, \boldsymbol{T}_2$ should act in the same point C_1 and C_2 , respectively:

$$\boldsymbol{r}_C = \boldsymbol{r}_{C_1} + \boldsymbol{r}_{C_2} \tag{10}$$

The unknowns of the problem for the short rotor case are the angle of rotation, ϕ, the magnitude of the normal, N and its direction, stipulated by the versor $\boldsymbol{u}_N$. The fact that the normal reaction N acts on a cylindrical surface makes that once the point of aplication C being stipulated, the direction of action is also defined.

2.2. Obtaining the Equations of Motion for the Case of a Short Rotor Actuated by Gravitational Force

A short rotor with a horizontal axis of rotation is presented in Figure 2. M is the mass of the rotor and J_{G_z} is the moment of inertia, with respect to a centroidal axis parallel to the axis of rotation. The motion of the rotor is ensured by a body of mass m, hung at the end of an inextensible wire winded on a cylinder of r radius.

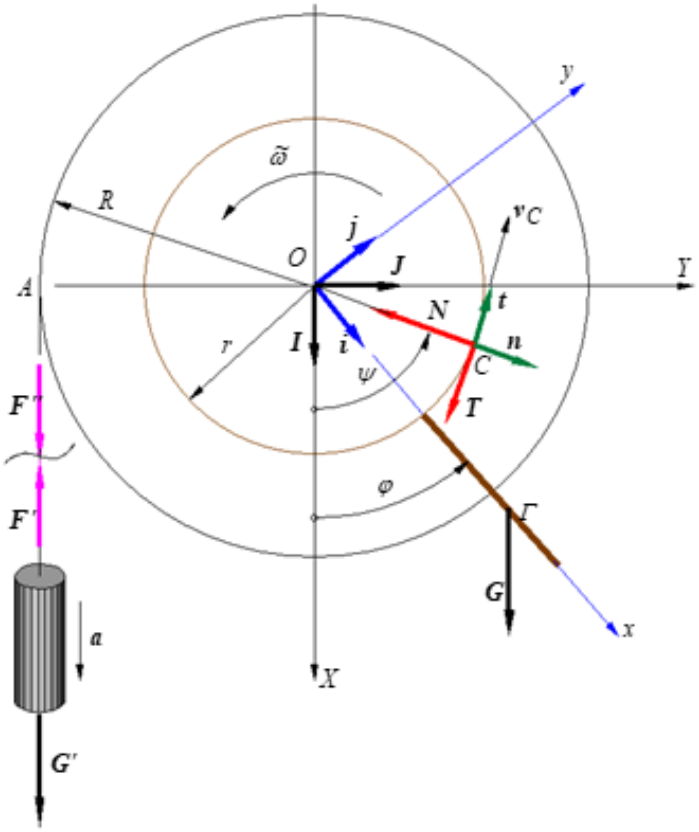

Figure 2. Short rotor actuated by gravitational force.

The hypothesis of dry friction, Coulomb type, existing in the bearing is accepted. Two situations are considered [40,41]:

- The friction is characterised exclusively by the coefficient of dynamic dry friction μ_d, model represented in Figure 3a:

$$\mu_1(v) = \mu_d \tag{11}$$

- The friction is characterised by both μ_d and the coefficient of static friction μ_s, model represented in Figure 3b:

$$\mu_2(v) = \begin{cases} \mu_d sign(v), |v| > v_{cr} \\ \frac{\mu_{st}}{v_{cr}} v, \left|v\right| \leq v_{cr} \end{cases} \tag{12}$$

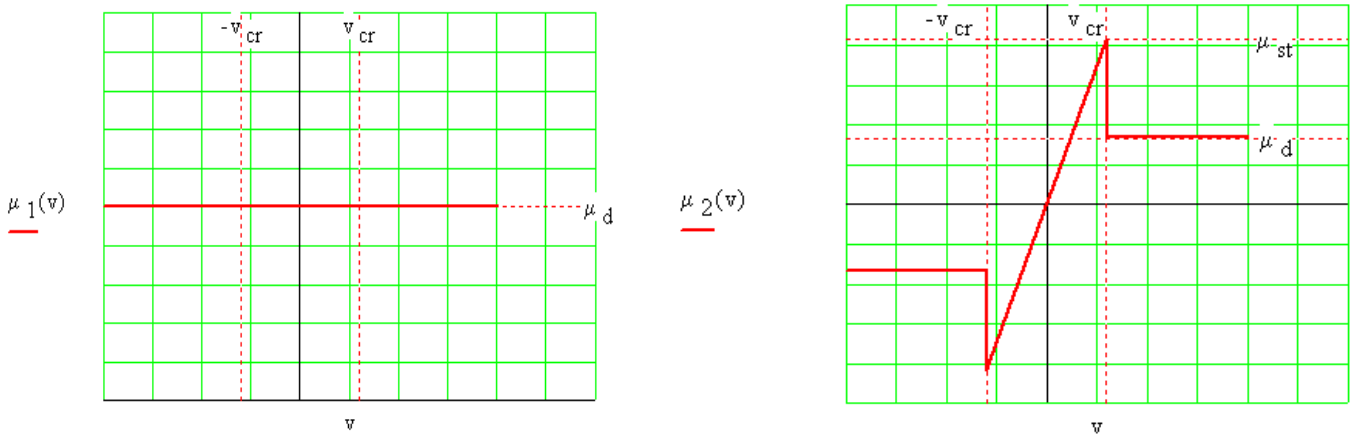

Figure 3. Representation of coefficient of friction for the cases considered: (**a**) dynamic friction: μ_d and (**b**) static and dynamic friction: μ_{st}, μ_d.

In the bearing of the rotor a system of normal elementary forces is developed that can be reduced to a normal reaction $\boldsymbol{N}$ which acts on the point C. For the normal reaction, neither the magnitude N nor the orientation—given by the angle ψ— are known. The presence of the normal reaction has an effect on the occurrence of the friction force $\boldsymbol{T}$, acting on the point C, and tangential to the cylindrical surface of the bearing of r radius. The direction of the friction force is opposite to the relative velocity $\boldsymbol{v}_C$ of the point C from the bearing and has the magnitude:

$$\boldsymbol{T} = -\mu(v_C)\frac{\boldsymbol{v}_C}{v_C}N \tag{13}$$

The rotor is set into motion by the suspended body but, from the free-body diagram, this is revealed by the tensions from the wire $\boldsymbol{F}'$ and $\boldsymbol{F}''$ to be occurring in a cross section, which must satisfy the condition:

$$\boldsymbol{F}' + \boldsymbol{F}'' = 0 \tag{14}$$

The equation of motion of the actuating body on the vertical direction is:

$$m\boldsymbol{a} = \boldsymbol{G}' - \boldsymbol{F}' \tag{15}$$

Since the wire is inextensible, the velocity of a point A from the periphery of the wiring cylinder must be equal to the downward velocity of the actuating body:

$$\dot{\varphi}R = v \tag{16}$$

The acceleration of the body in downward motion is found by the derivative with respect to time of relation (16):

$$\ddot{\varphi}R = a \tag{17}$$

As shown previously, the mass centre theorem and the angular momentum theorem with respect to the centre of mass should be applied [42]; to this purpose definitions of the versors are required:

- the versors of the immobile reference system $\boldsymbol{I}, \boldsymbol{J}, \boldsymbol{K}$:

$$\boldsymbol{I} = \begin{bmatrix} 1 \\ 0 \\ 0 \end{bmatrix}, \boldsymbol{J} = \begin{bmatrix} 0 \\ 1 \\ 0 \end{bmatrix}, \boldsymbol{K} = \begin{bmatrix} 0 \\ 0 \\ 1 \end{bmatrix} \tag{18}$$

- the versors of the mobile frame, $\boldsymbol{i}, \boldsymbol{j}, \boldsymbol{k}$ expressed via the projections on the axes of the fixed frame:

$$\boldsymbol{i} = \begin{bmatrix} cos\varphi \\ sin\varphi \\ 0 \end{bmatrix}, \boldsymbol{j} = \begin{bmatrix} -sin\varphi \\ cos\varphi \\ 0 \end{bmatrix}, \boldsymbol{k} = \boldsymbol{K} \tag{19}$$

- and the versors of the normal and tangent direction to the surface of the bearing in the contact point, $\boldsymbol{n}$ and $\boldsymbol{t}$, respectively:

$$\boldsymbol{n} = \begin{bmatrix} cos\psi \\ sin\psi \\ 0 \end{bmatrix}, \boldsymbol{t} = \begin{bmatrix} -sin\psi \\ cos\psi \\ 0 \end{bmatrix}, \tag{20}$$

The mass centre theorem has the form:

$$M\boldsymbol{a}_\Gamma = \boldsymbol{G} + \boldsymbol{N} + \boldsymbol{T} + \boldsymbol{F}'' \tag{21}$$

where the terms from relation (21) are explained by the following relations:

$$\boldsymbol{a} = -\dot{\varphi}^2 x_M \boldsymbol{n} + \ddot{\varphi} x_M \boldsymbol{t} \tag{22}$$

$$\boldsymbol{G} = Mg\boldsymbol{I} \tag{23}$$

$$\boldsymbol{N} = -\boldsymbol{n}N \tag{24}$$

$$\boldsymbol{T} = -\mu N sign(\dot{\varphi} r)\boldsymbol{t} \tag{25}$$

$$\boldsymbol{F}'' = F'\boldsymbol{I} = m(g - R\ddot{\varphi})\boldsymbol{I} \tag{26}$$

In relation (25), the $sign(x)$ represents the *signum* function, defined as:

$$sign(x) = \begin{cases} 1, x > 0 \\ -1, x < 0 \\ 0, x = 0 \end{cases} \tag{27}$$

After expressing all vectors from Equation (21) as functions of the versors of the fixed system, two scalar equations are obtained:

$$\begin{cases} -M\dot{\varphi}^2 x_M cos\varphi - M\ddot{\varphi} x_M sin\varphi + Ncos\psi - \mu N sin\psi \; sign(\dot{\varphi}) - (M+m)g + mR\ddot{\varphi} = 0 \\ -M\dot{\varphi}^2 x_M sin\varphi + M\ddot{\varphi} x_M cos\varphi + Nsin\psi + \mu N cos\psi \; sign(\dot{\varphi}) = 0 \end{cases} \tag{28}$$

The scalar Equation (28) is obtained by projecting a plane vector equation on the axes of a Cartesian system; by multiplying the second equation by the imaginary i, ($i^2 = -1$), and summing the equations member by member, the equation can be approached unitary as

is shown in [43]. Considering Euler's formula, $\cos\varphi + i\sin\varphi = \exp(i\varphi)$, a unique equation is obtained, in the unknown the φ angle.

The angular momentum theorem with respect to the centre of mass has the form:

$$J_{Gz}\ddot{\varphi}\boldsymbol{k} = \bar{\Gamma C} \times (\boldsymbol{N} + \boldsymbol{T}) + \bar{\Gamma A} \times \boldsymbol{F''} \tag{29}$$

where:

$$\Gamma C = -x_M \boldsymbol{i} \tag{30}$$

$$\bar{\Gamma A} = -x_M \boldsymbol{i} + (-R)\boldsymbol{J} \tag{31}$$

Based on relations (24), (25), (27), (28) and (29), a unique vector equation results, that has projection only on the direction of the axis of rotation:

$$\begin{array}{l} \left(J_{Gz} + mR^2 + mRx_M sin\varphi\right)\ddot{\varphi} + \left[sin\varphi - \mu cos\varphi\ sign\left(\dot{\varphi}\right)\right]x_M N cos\varphi \ldots \\ -\left(cos\varphi + \mu sin\varphi\ sign\left(\dot{\varphi}\right)\right)x_M N sin\psi - m(R + x_M sin\varphi)g + \mu rN\ sign\left(\dot{\varphi}\right) = 0 \end{array} \tag{32}$$

Equations (28) and (32) create a system that has as unknowns the angle of rotation of the rotor, φ, the magnitude of the normal reaction N and the angle ψ that stipulates the position of the normal reaction. In order to solve this system, one can notice that Equation (28) is linear with respect to $cos\psi$ and $sin\psi$; this is a fact that suggests the introduction of the new variables:

$$X = Ncos\psi;\ Y = Nsin\psi \tag{33}$$

The system takes the form:

$$\left\{\begin{array}{l} X - \mu Y sign\left(\dot{\varphi}\right) = (M+m)g - mR\ddot{\varphi} + M\dot{\varphi}^2 x_M cos\varphi + M\ddot{\varphi}x_M sin\varphi \\ \mu X sign\left(\dot{\varphi}\right) + Y = M\dot{\varphi}^2 x_M sin\varphi - M\ddot{\varphi}x_M cos\varphi \\ \left(J_{Gz} + mR^2 + mRx_M sin\varphi\right)\ddot{\varphi} + \left[sin\varphi - \mu cos\varphi\ sign\left(\dot{\varphi}\right)\right]x_M X \ldots \\ -\left(cos\varphi + \mu sin\varphi\ sign\left(\dot{\varphi}\right)\right)x_M Y - m(R + x_M sin\varphi)g + \mu rN sign\left(\dot{\varphi}\right) = 0 \end{array}\right. \tag{34}$$

From the first two equations of system (34) we obtain:

$$\left\{\begin{array}{l} X = \frac{sin\varphi - \mu cos\varphi\ sign\left(\dot{\varphi}\right) - \frac{mR}{Mx_M}}{1+\mu^2} Mx_M\ddot{\varphi} + \frac{\mu sin\varphi\ sign\left(\dot{\varphi}\right) + cos\varphi}{1+\mu^2} Mx_M\dot{\varphi}^2 + \frac{M+m}{1+\mu^2}g \\ Y = -\frac{cos\varphi - \mu sign\left(\dot{\varphi}\right)\left(\frac{mR}{Mx_M} - sin\varphi\right) -}{1+\mu^2} Mx_M\ddot{\varphi} + \frac{sin\varphi - \mu cos\varphi sign\left(\dot{\varphi}\right)}{1+\mu^2} Mx_M\dot{\varphi}^2 - \mu\frac{M+m}{1+\mu^2}gsign(\dot{\varphi}) \end{array}\right. \tag{35}$$

and from relations (33):

$$N = \sqrt{X^2 + Y^2} \tag{36}$$

The last equation of the system (34) takes the form:

$$\begin{array}{l} \left(J_{Gz} + mR^2 + mRx_M sin\varphi\right)\ddot{\varphi} + \left[sin\varphi - \mu cos\varphi\ sign\left(\dot{\varphi}\right)\right]x_M X \ldots \\ -\left(cos\varphi + \mu sin\varphi\ sign\left(\dot{\varphi}\right)\right]x_M Y - m(R + x_M sin\varphi)g + \mu r\left(\sqrt{X^2 + Y^2}\right)\ sign\left(\dot{\varphi}\right) = 0 \end{array} \tag{37}$$

Equation (37) is an irrational one, with the unknowns the angle of rotation of the rotor, ϕ and its derivatives, $\dot{\varphi}$ and $\ddot{\varphi}$. In order to resolve this equation, the term containing the root $\sqrt{X^2 + Y^2}$ is isolated in the right member and then, both sides of the equation are squared. An equation of second order in unknown $\ddot{\varphi}$ is obtained, which has the solutions:

$$\ddot{\varphi}_{1,2} = \frac{-B \pm \sqrt{B^2 - AC}}{A} \tag{38}$$

where

$$\begin{cases} A = (J_{Gz} + mR^2 + Mx_M^2)^2 - \mu^2 r^2 \frac{M^2 x_M^2 - 2mMx_M R + m^2 R^2}{1+\mu^2} \\ B = \left(J_{Gz} + mR^2 + Mx_M^2\right)(x_M M sin\varphi - mR)g + \\ \frac{\mu^2}{1+\mu^2} r^2 \left[MmRx_M \dot{\varphi}^2 cos\varphi - [Mx_M sin\varphi + mR](M+m)g\right] \\ C = (x_M M sin\varphi - mR)^2 g^2 + \\ \frac{\mu^2}{1+\mu^2} r^2 \left[M^2 x_M^2 \dot{\varphi}^4 + 2M(M+m)x_M \dot{\varphi}^2 g cos\varphi + (M+m)^2 g^2\right] \end{cases} \quad (39)$$

2.3. Integration of the Equations of Motion for the Case of Short Rotor

2.3.1. The Motion of the Rotor

Analysing Equations (38) and (39) it can be observed that the motion of the rotor is described by a strongly nonlinear differential equation. In order to integrate it, the Runge–Kutta IV algorithm [44] was applied. Additionally, by squaring the equation for radical elimination, an extraneous root was introduced which should be ignored. For a set of typical values $J_{Gz} = 0.012$ kg · m^2; $\mu_d = 0.5$; $r = 0.006$ m; $M = 1.2$ kg; $x_M = 0.1$ m; $R = 0.02$ m; $m = 0.3$ kg and for the initial conditions:

$$t = 0, \begin{cases} \varphi = \varphi_0 = \pi/2 \\ \omega = \omega_0 = 0 \end{cases} \quad (40)$$

the results of the integration of differential Equation (38) are plotted in Figure 4. The plots from Figure 4 do not correspond to physical reality, since for the considered value of the coefficient of friction, $\mu_d = 0.5$, the amplitude of the oscillations does not decrease but instead remains constant for Equation (38).

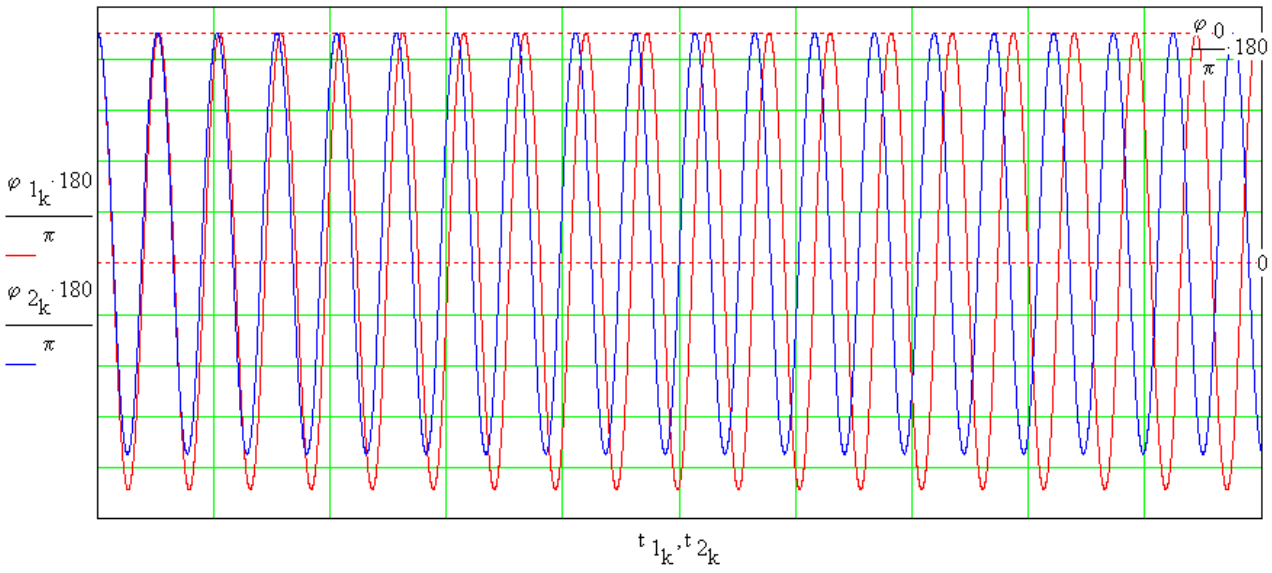

Figure 4. The angle of rotation of the rotor, obtained by numerical integration of the equations of motion: $\varphi_{1,2}$—the solutions of Equation (38).

In [45] it was shown that a correction must be applied to the Equation (38), under the form:

$$\ddot{\varphi}_{1,2} = \frac{-B \pm \sqrt{B^2 - AC} sign(\dot{\varphi})}{A} \quad (41)$$

The function $sign(\dot{\varphi})$ was introduced because it disappeared when Equation (38) was squared for removing the radical, with the consequence:

$$sign(x)^2 = 1. \quad (42)$$

Integrating once more the two equations, one can state the correct solution:

$$\ddot{\varphi}_1 = \frac{-B - \sqrt{B^2 - AC}sign(\dot{\varphi})}{A} \tag{43}$$

The attempt to integrate the other option:

$$\ddot{\varphi}_2 = \frac{-B + \sqrt{B^2 - AC}sign(\dot{\varphi})}{A} \tag{44}$$

conducts to the blocking of the programme for a very small value of the sample time since the angular velocity of the rotor increases very rapidly. In Figure 5 there are presented comparatively the variations of angular velocity corresponding to Equation (43), red line, and Equation (44), blue line, when only the dynamic friction was supposed, characterised by a coefficient of friction $\mu_d = 0.5$. One can remark that Equation (43) models a damped oscillatory motion while Equation (44) suggests a rotational motion with the angular velocity increasing rapidly.

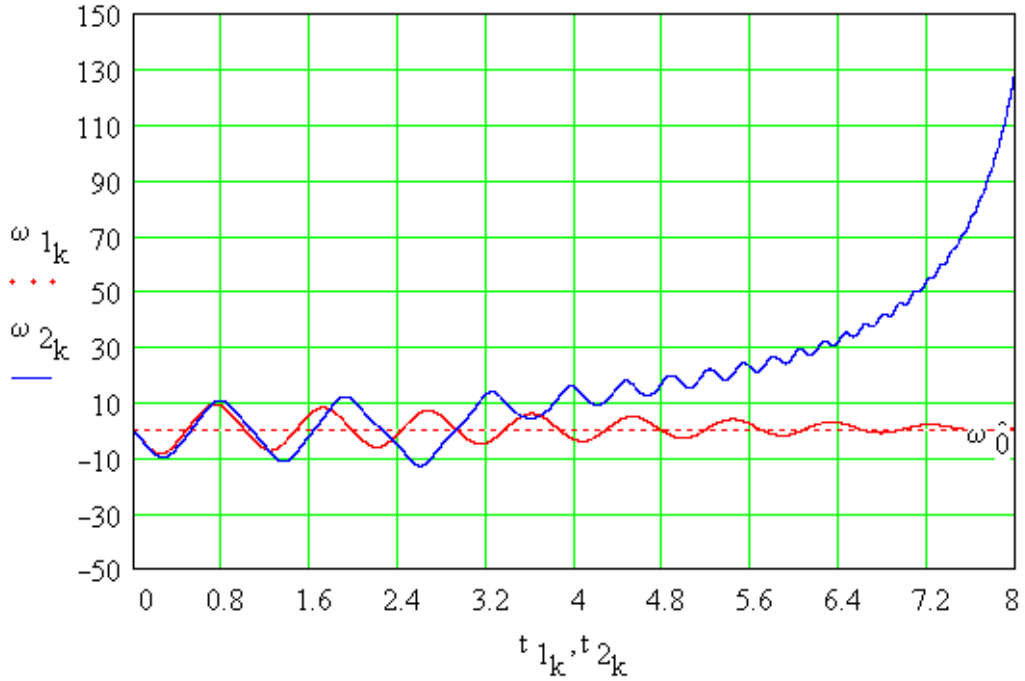

Figure 5. Variation of the angular velocity of the rotor according to Equation (39), red line, and Equation (40), blue line, for $\mu_d = 0.5$.

In order to eliminate any indecision, Equations (43) and (44) were integrated for two values of the coefficient of friction; the variations of the angular velocities of the rotor are represented in Figure 6. From Figure 6b one can observe that Equation (44) foresees a rotational motion, with the angular velocity increasing more rapidly with increased friction, while Equation (43), (Figure 6a), predicts an oscillatory motion with decreasing amplitude for greater value of the coefficient of friction. From here, we draw the conclusion that Equation (43) corresponds to physical reality.

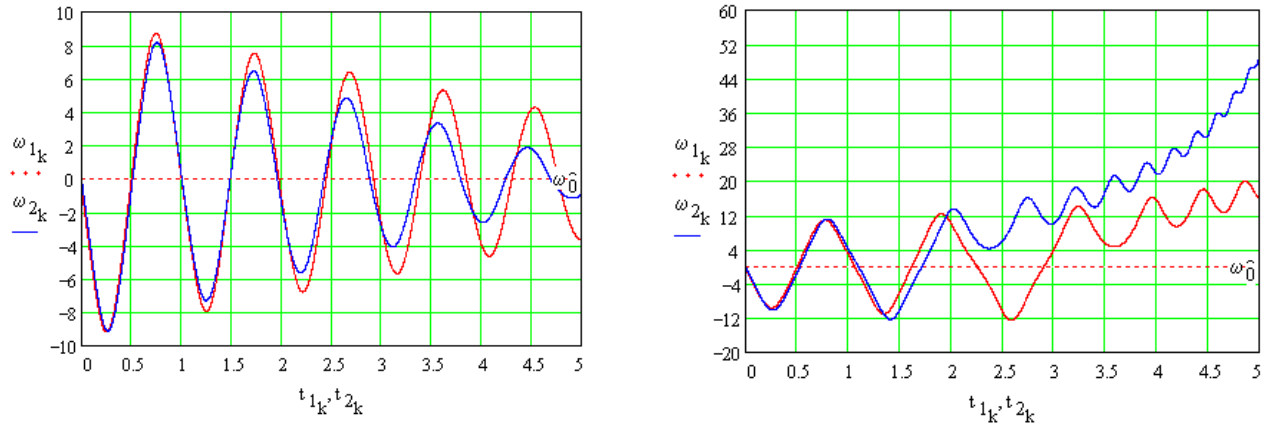

(**a**) (**b**)

Figure 6. The variation of the angular velocity of the rotor for two values of the coefficient of friction, $\mu_{d1} = 0.5$ (red line) and $\mu_{d2} = 0.9$ (blue line), for (**a**) solution according to Equation (43) and (**b**) solution according to Equation (44).

Next, for a set of mechanical parameters: $M = 0.5$ kg; $J_{Gz} = 0.012$ kg $\cdot$ m^2; $m = 0.3$ kg; $r = 0.006$ m and $R = 0.02$ m, we studied the influence of the coefficient of friction and of the eccentricity upon the angular velocity of the rotor for the initial conditions:

$$\varphi(t = 0) = \pi;\ \omega(t = 0) = 0 \tag{45}$$

The variation of the angular velocity, obtained with the relation (32), for a balanced rotor, for two different values of the coefficient of friction is presented in Figure 7.

The plots show that the angular velocity increases linearly with time, according to the analytic study, and the higher the coefficient of friction, the lesser the increase of velocity, Figure 7a. The effect of eccentricity of the rotor in the absence of friction is presented in Figure 7b; the angular velocity oscillates about a mean value that increases continuously and the average value of velocity increases more rapidly for a smaller eccentricity. In Figure 7c the effect of the coefficient of friction upon the velocity of two rotors with identical eccentricities and a clear different dynamic behaviour is observed; the first rotor presents a continuous rotational motion and tends to oscillate about a constant value, but the motion of the second rotor stops after a relatively short time. Lastly, the cumulative effect of friction and eccentricity is presented in Figure 7d. It can be noticed that for a minor friction, even for a substantial increase of eccentricity $x_m = 0.6$ m, the rotor will still be in motion, but for high friction $\mu = 0.7$ and small eccentricity the motion of the rotor stops.

An interesting feature is the effect of the value of the velocity at which the transition from static to dynamic friction occurs. In Figures 8 and 9 the variation of angular velocity for different values of transition velocity v_{cr} is presented for the initial conditions (45) and (46), respectively:

$$\varphi(t = 0) = \varphi_0 = \pi/2;\ \omega(t = 0) = \omega_0 = 0 \tag{46}$$

When the rotor is set to motion from rest for $\varphi_0 = \pi$ for reduced values of transition velocity ($v_{cr} = 0.01$ m/s) the effect of v_{cr} is not perceptible and the plots are quasi identical, as shown in Figure 8a. For increased transition velocity ($v_{cr} = 0.1$ m/s), the motion is rotational but the angular velocity for the rotor with static friction (blue line) is smaller. Increasing again the transition velocity to $v_{cr} = 0.5$ m/s the motions are both rotational but the angular velocity for the rotor with static and dynamic friction (blue line) is greater than for the rotor with dynamic friction (red line).

In Figure 9 the same variations as in Figure 8 are presented, but for a different launching of the initial conditions (46). This time, regardless of the values of the coefficients of friction and of the adopted friction model, the rotor presents a linearly damped oscillatory

motion, with a pronounced damping for the case when only dynamic friction is considered. The model considering both static and dynamic friction shows a diminished damping velocity when the transition velocity increases.

The analysis of the evolution of the dynamic system reveals that when both friction and eccentricity are present, the rotor may perform either a linearly damped oscillatory motion or a rotational motion with the angular velocity varying about a constant value. For a set of constructive values and magnitudes of tribological parameters, the factors determining the evolution of the system in one manner or another, are expected to be the values of the initial position φ_0 and initial angular velocity ω_0.

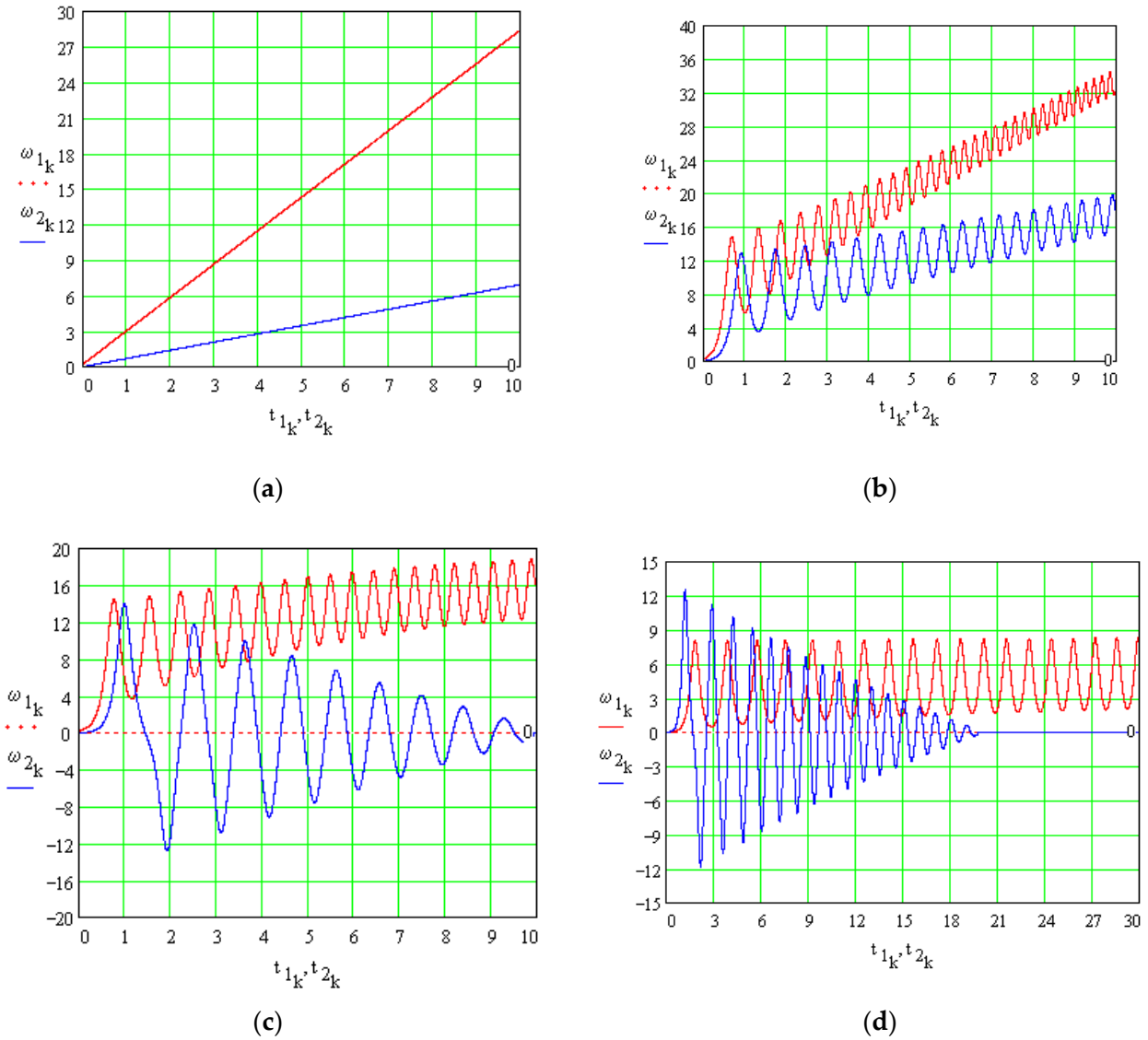

Figure 7. The effect of dynamic friction and eccentricity upon the angular velocity of the rotor: (**a**) the effect of friction upon the angular velocity for a balanced rotor $\mu_1 = 0.3$, (red), $\mu_2 = 0.7$, (blue), $x_{M_1} = x_{M_2} = 0$; (**b**) the effect of eccentricity upon the angular velocity for unbalanced rotor, $\mu_1 = 0.0$, $\mu_2 = 0$, $x_{M1} = 0.1$ m, (red), $x_{M_2} = 0.2$ m(blue); (**c**) the cumulative effect of friction and eccentricity upon the angular velocity—two identical eccentric rotors, different coefficients of friction $\mu_1 = 0.3$, (red), $\mu_2 = 0.7$, (blue); $x_{M_1} = x_{M_2} = 0.1$ and (**d**) the cumulative effect of friction and eccentricity upon the angular velocity—eccentric rotors, different coefficients of friction $\mu_1 = 0.3$, $x_{M_1} = 0.6$ m (red); $\mu_2 = 0.7$, $x_{M_2} = 0.2$ m (blue).

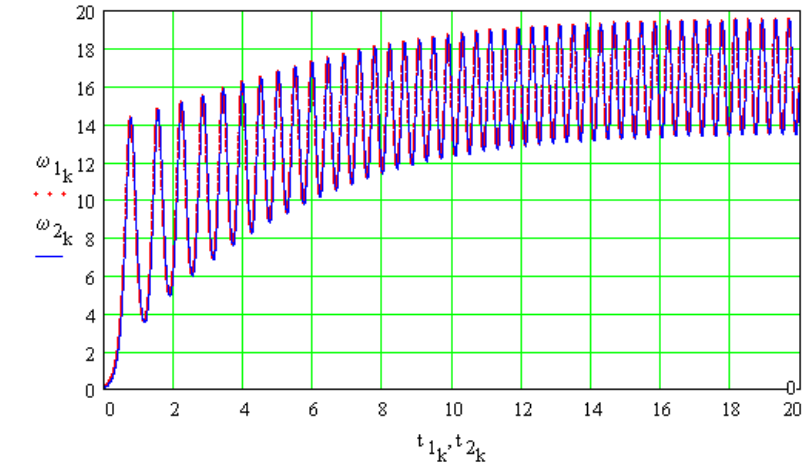

(**a**)

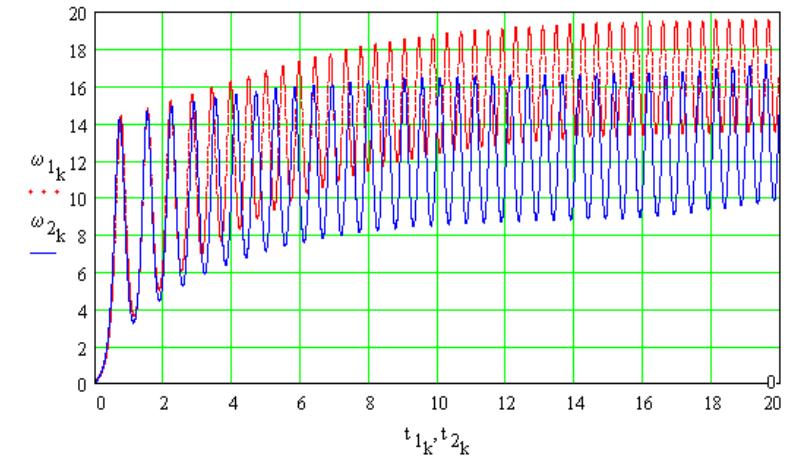

(**b**)

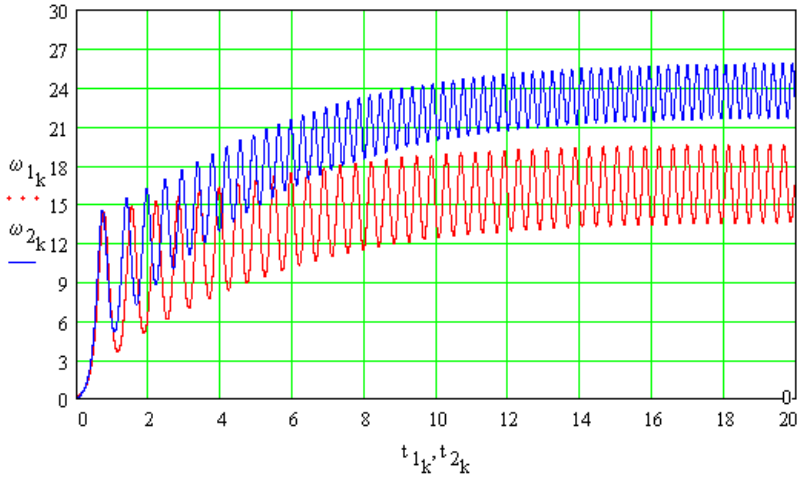

(**c**)

Figure 8. The effect of transition velocity v_{cr} upon the rotors' dynamics for initial conditions $\varphi_0 = \pi$; $\omega_0 = 0$, when different friction models are considered: dynamic friction (red line), $\mu_d = 0.3$; static and dynamic friction (blue line), $\mu_{st} = 0.5$, $\mu_d = 0.3$: (**a**) $v_{cr} = 0.01$ m/s; (**b**) $v_{cr} = 0.1$ m/s and (**c**) $v_{cr} = 0.5$ m/s.

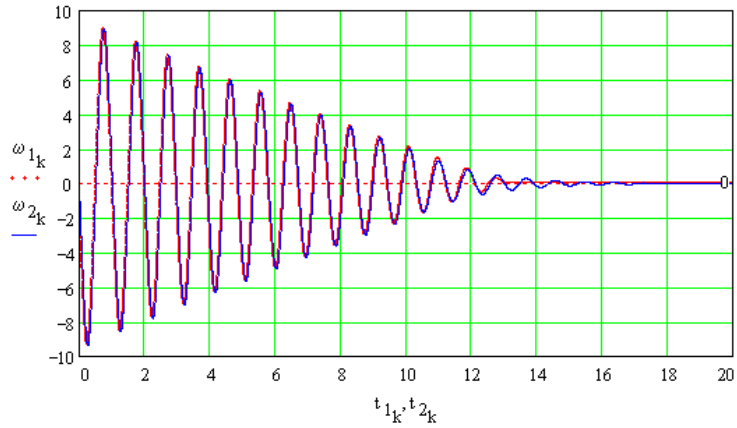

(**a**)

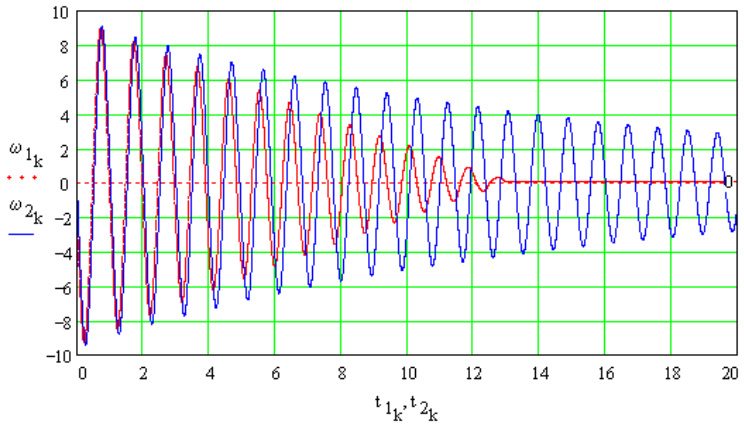

(**b**)

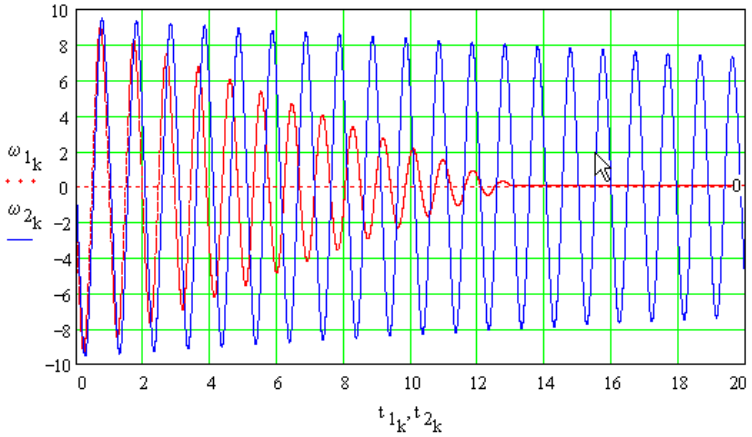

(**c**)

Figure 9. The effect of transition velocity v_{cr} upon the dynamics of the rotor when dynamic friction (red line) and static plus dynamic friction (blue line) is considered, for the initial conditions $\varphi_0 = \frac{\pi}{2}$; $\omega_0 = 0$. (**a**) $v_{cr} = 0.01$ m/s; (**b**) $v_{cr} = 0.1$ m/s and (**c**) $v_{cr} = 0.5$ m/s.

In Figure 10 the variation of the angular velocity of the rotor launched from rest is presented for different values of the angle φ_0 varying in a very narrow range, for the transition velocity varying in a large domain. It is observed that the theoretical model predicts the existence of a well-stipulated launching angle that delimitates the two domains

of evolution of the system, while the change of the transition velocity does not alter qualitatively the type of motion of the system (from oscillatory to rotational and reverse) but only modifies the kinematic parameters (amplitude, period, average velocity, etc.).

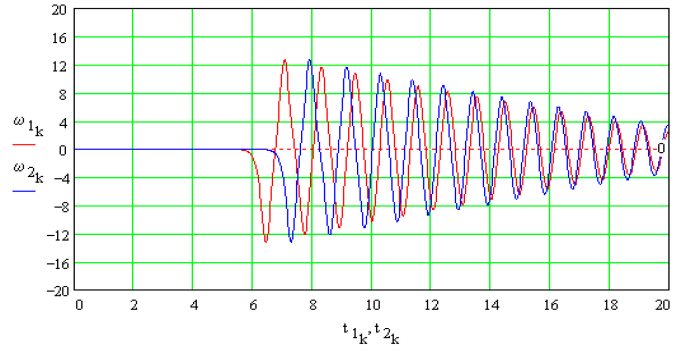

(**a**)

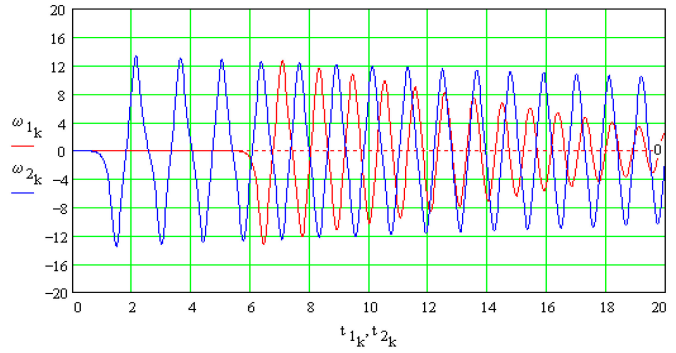

(**b**)

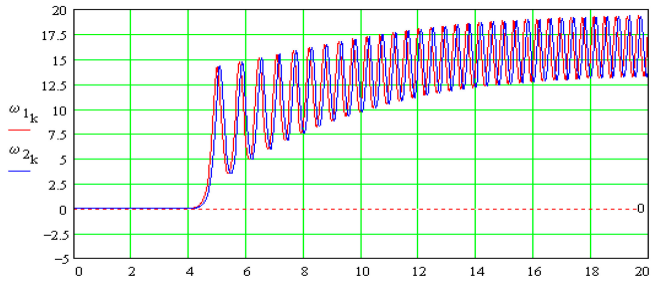

(**c**)

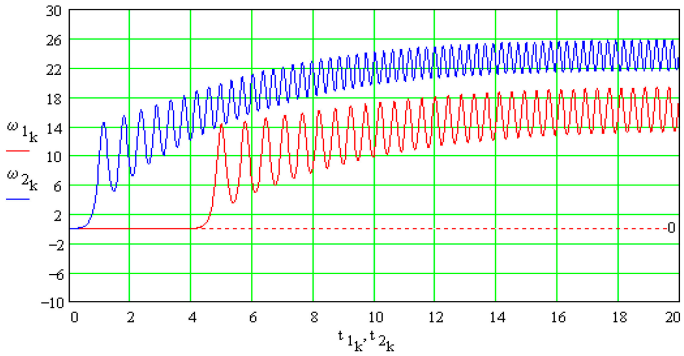

(**d**)

Figure 10. Variation of angular velocity of the rotor, for dynamic friction model (red plot) and static-and dynamic friction model (blue plot): (**a**) $v_{cr} = 0$; $\varphi_0 = 0.984\pi$; (**b**) $v_{cr} = 0.5\ \frac{\mathrm{m}}{\mathrm{s}}$; $\varphi_0 = 0.984\pi$; (**c**) $v_{cr} = 0$, $\varphi_0 = 0.985\pi$ and (**d**) $v_{cr} = 0.5\frac{\mathrm{m}}{\mathrm{s}}$; $\varphi_0 = 0.985\pi$.

Figure 11 highlights the complexity of the analysed system. In this figure, the effects of the initial angular velocity and friction hypothesis are presented. In Figure 11a, the energy of the rotor is bigger than the energy of the rotor represented in Figure 11c, but at the end, the rotor is at rest for the first case, while for a smaller value, last case, the rotor remains in steady motion. Another remark results from Figure 11b, where the two laws of friction determining completely different dynamic behaviours.

2.3.2. Finding the Normal Reaction from the Bearing of the Rotor

With the law of motion $\varphi = \varphi(t)$, known from the integration of Equation (43), one can find, using the relations (35), the projections on the axes of the immobile system of the normal $N : X = X(t)$, $Y = Y(t)$ and from here, the angle $\psi(t)$ that the direction of the normal N makes with the OX axis.

$$\psi(t) = angle[X(t), Y(t)] \tag{47}$$

The inverse function of two arguments was the option because the use of the function (y/x) would create confusions; for different positions of the normal reaction, the same value of the angle ψ is obtained:

$$atan(y/x) = atan(-y/-x) \tag{48}$$

For a stipulated position of the direction of the normal, the relation (47) gives a single angle from the interval $[0, 2\pi]$, while the relation (48) gives two values for the angle from the same interval.

In Figure 12 there are represented comparatively the results obtained with Equations (47) and (48). For the dynamic friction model, Figure 12a, the variation in time of the angles of reactions are plotted in Figure 12c, and the correct one is represented blue, obtained with relation (47) while the red plot, obtained with relation (48), is not valid. In Figure 12e, the angular velocity of the rotor (blue plot) is compared to the angular velocity of the direction of reaction (red plot). The friction model that considers both static and dynamic friction is analysed in Figure 12b,d,f: variation of the angles of reactions in Figure 12 (in blue, the solution from Equation (47) and red plot, solution from Equation (48)) and the variation of the angular velocities, for rotor (blue plot) and reaction (red plot), in Figure 12f.

In Figure 13, similarly to Figure 12 but for initial launching conditions $\varphi_0 = \pi/2$, $\omega_0 = 0$, there are evidenced the angles of reactions and the angular velocities for the two friction models, with the comparison between the solutions obtained with the adequate relation (47) and the improper relation (48).

The variations of the normal reactions for the two friction models N_1, N_2 are represented in Figure 14 for $\varphi_0 = \pi$ and in Figure 15 for $\varphi_0 = \pi/2$. The corresponding friction forces T_1, T_2 are also plotted in these figures. To be remarked from Figure 15b that the two friction models predict for the friction forces complete different variations: for the friction model from Figure 13a (only dynamic friction) the friction force from the bearing, T_1, presents discontinuities and jumps from positive to negative values but for the model with static friction (Figure 13b) the friction force T_2 has continuous variation.

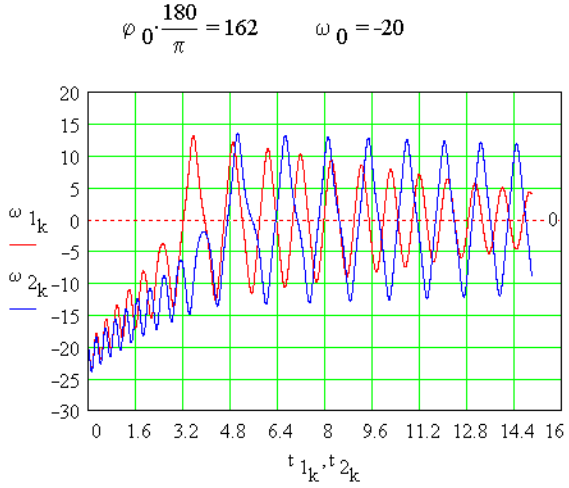

(**a**)

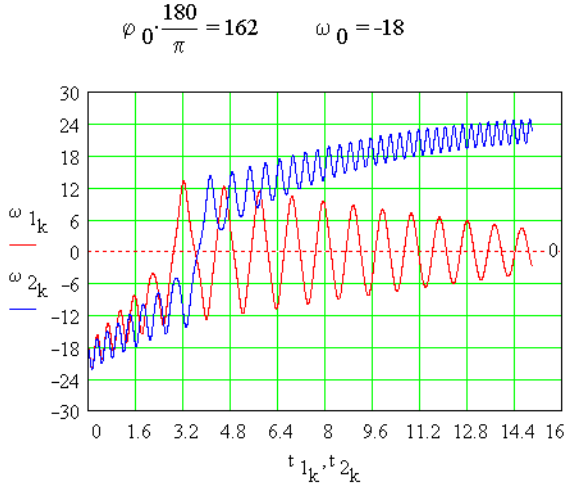

(**b**)

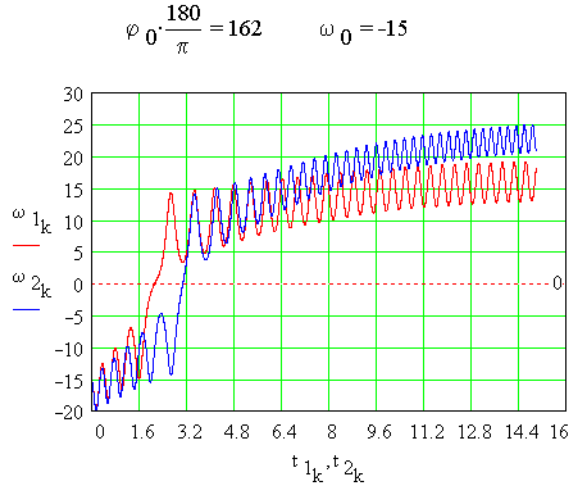

(**c**)

Figure 11. The effect of the initial conditions (angular velocity) and the friction force model upon the system evolution: (**a**) $\varphi_0 = 162$ deg, $\omega_0 = -20\frac{\text{rad}}{\text{s}}$; (**b**) $\varphi_0 = 162$ deg, $\omega_0 = -18\frac{\text{rad}}{\text{s}}$; (**c**) $\varphi_0 = 162$ deg, $\omega_0 = -15$ rad/s..

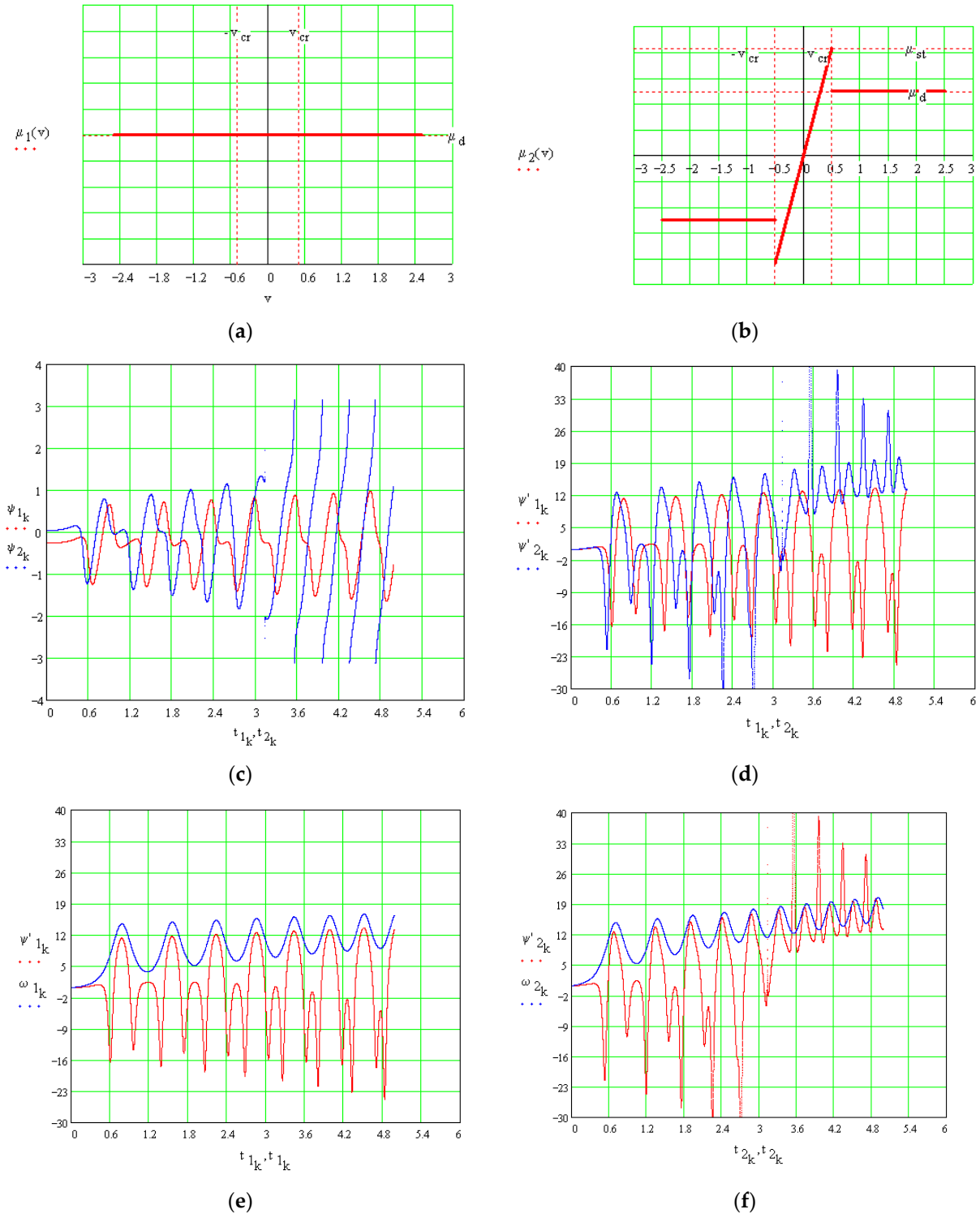

Figure 12. Comparison between the analytical solutions of the angles of reaction and angular velocities for the two friction models, launching for initial conditions $\varphi_0 = \pi$: (**a**) dynamic friction model; (**b**) static and dynamic friction model; (**c**) angles of the reactions for model from (**a**); (**d**) angles of the reactions for the model from (**b**); (**e**) angular velocity of the rotor and of the direction of the reaction, model from (**a**); (**f**) angular velocity of the rotor and of the direction of the reaction, model from (**b**).

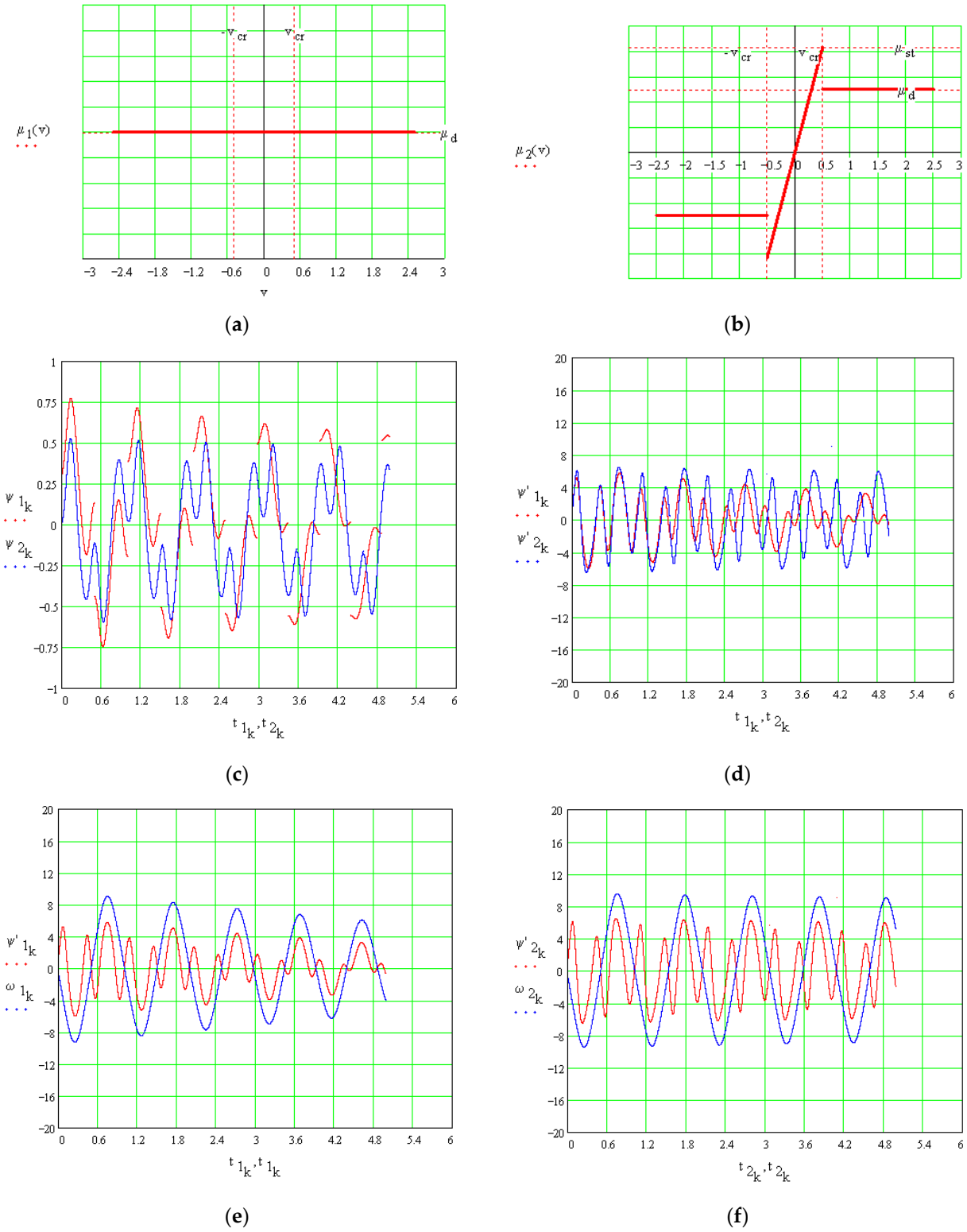

Figure 13. Launching for $\varphi_0 = \pi/2, \omega_0 = 0$: (**a**) dynamic friction model; (**b**) static and dynamic friction model; (**c**) angles of the reactions for model from (**a**); (**d**) angles of the reactions for the model from (**b**); (**e**) angular velocity of the rotor and of the direction of the reaction, model from (**a**); **(f)** angular velocity of the rotor and of the direction of the reaction, model from (**b**).

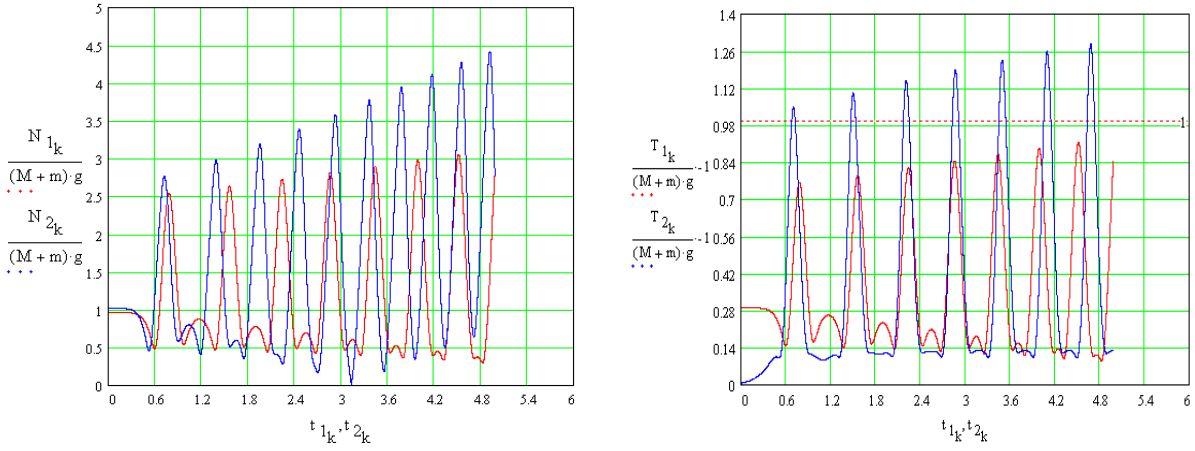

(**a**) (**b**)

Figure 14. Forces from the plain bearing for the two friction models, for $\varphi_0 = \pi$: (**a**) the normal reactions $N_1,\ N_2$; (**b**) the friction forces $T_1,\ T_2$; (red, dynamic friction; blue, static and dynamic friction).

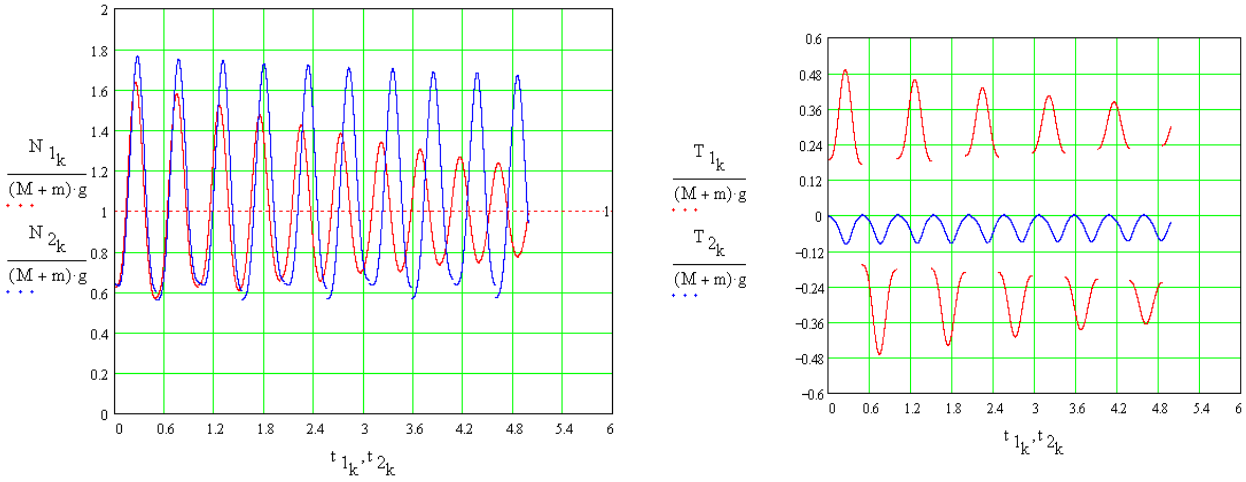

(**a**) (**b**)

Figure 15. Forces from the bearing for $\varphi_0 = \pi/2$: (**a**) the normal reactions $N_1,\ N_2$; (**b**) the friction forces $T_1,\ T_2$; (red, dynamic friction; blue, static and dynamic friction).

3. Experimental Corroboration

3.1. The Experimental Device

In order to validate the theoretical results obtained, a device was designed and constructed, Figure 16. The rotor consists in a bronze bushing 1, inner diameter $2r = 10$ mm and length 40 mm. The bushing is pressed mounted into a central hole of an aluminium prismatic bar 2. Two symmetrical holes are made into the bar 2, where two aluminium discs, 3 and 4, are mounted with two screws, 5. The disc 3 has the mass $m_1 = 0.2$ kg and the disc 4 has the mass $m_2 = 0.1$ kg. The parts 1–5 form the asymmetric rotor. Modifying the order of assembling the discs into the two holes, only the eccentricity x_M of the rotor varies, the other inertia characteristics (the mass M and the moment of inertia with respect to the axis of rotation) remain unchanged. The rotor is assembled on the fixed shaft 7 with the possibility of rotating about the shaft. To launch the rotor into motion, an inextensible wire is winded on the outer surface of the bushing having suspended at the other end the actuating part 8 of mass m.

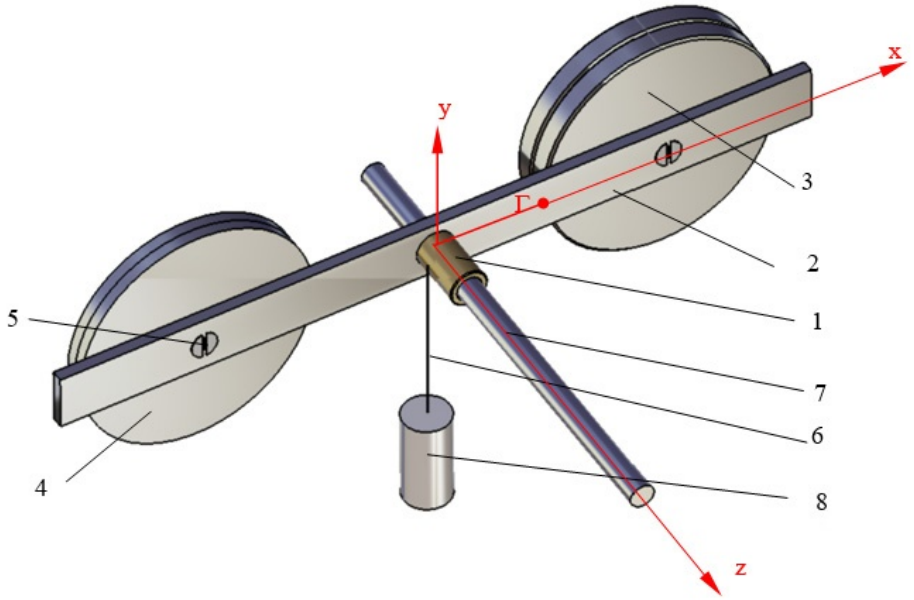

Figure 16. Sketch of the laboratory device: 1—bushing; 2—rod; 3 and 4—discs; 5—screw, 6—inextensible wire, 7—shaft, 8—cylindrical part.

The angular velocity is difficult to measure accurately; therefore, it is preferred that the rotor is launched from rest but for varying launching angles. The reference coordinate system of the rotor $Oxyz$ is similar to the theoretical one, the Oz axis is the axis of rotation, the Ox axis passes through the center of mass Γ and the Oy axis competes the right frame.

The rotor was modelled in CATIA, software allowing for the estimation of inertial characteristics. In Figure 17 a capture is presented with the window showing the obtained inertial characteristics of the rotor.

Result

Calculation mode : Exact

Type : Volume

Characteristics		Center Of Gravity (G)	
Mass	0,788kg	Gx	37,492mm
		Gy	-1,113e-008mm
		Gz	-5,968mm

Inertia / G | Inertia / O | Inertia / P | Inertia / Axis | Inertia / Axis System

Inertia Matrix / G

IoxG	4,522e-004kgxm2	IoyG	0,009kgxm2	IozG	0,009kgxm2
IxyG	7,241e-013kgxm2	IxzG	2,251e-004kgxm2	IyzG	-3,539e-014kgxm2

Principal Moments / G

M1	4,463e-004kgxm2	M2	0,009kgxm2	M3	0,009kgxm2

Principal Axes

A1x	0,999653	A2x	0	A3x	0,02636
A1y	0	A2y	-1	A3y	0
A1z	-0,02636	A2z	0	A3z	0,999653

Figure 17. Finding the inertial characteristics of the rotor by CATIA model.

From Figure 17 there are retained: moment of inertia $J_{G_z} = 0.009$ kg $\cdot$ m^2; position of the center of mass $x_M = 37.5$ mm and mass of the rotor $M = 0.788$ kg. It also can be observed that the centrifugal products J_{xy} and J_{yz} are zero due to the fact that the plane xz is the plane of symmetry of the rotor. Additionally, the centroidal moment of inertia with respect to the axis parallel to the axis of rotation $J_{Gz} = 9 \cdot 10^{-3}$ kg $\cdot$ m^2 while the centrifugal product $J_{xz} = 2.25 \cdot 10^{-4}$ kg $\cdot$ m^2 is practically 2.5% of J_{Gz}, and can be neglected. Thus, the conditions to assimilate the proposed system to a short rotor, relation (8), are fulfilled. The laboratory device constructed according to the sketch from Figure 16 is presented in Figure 18.

Figure 18. The laboratory set up.

The principle of validation of the theoretical model consists in comparing the law of motion of the theoretical model to the one of the physical rotor. The motion of the experimental device was established via a non-contact method, applied in order to minimize the measuring errors. To this end, a graduated disc was attached to the prismatic bar. The wire was wound on the bronze bushing and the arm of the rod containing the centre of mass Γ was brought into the desired launching position, the angle φ_0 being measured with respect to the downward vertical. The system is released, and the entire motion of the system is video recorded, using a camera with an acquisition velocity of 240 $frames/sec$. Using specialised software, the index j of a frame corresponding to a mark from the graduated disc is found and then the numerical dependency between the values of the angle of rotation and time is obtained:

$$\varphi_{ex_j} = j\Delta\varphi \tag{49}$$

where $\Delta\varphi$ is the angular increment $\Delta\varphi = \pi/4 rad$ and the time corresponding to a rotation of angle φ_{ex_j} is:

$$t_{ex_j} = \frac{frame_j - frame_0}{240 \cdot frame/sec} \tag{50}$$

In order to compare the experimental data to the theoretical data, finding the coefficient of friction is necessary. A first method is to use the values of the coefficients μ_{st} and μ_d from the literature [46]. Another precise and rapid method to find the dynamic coefficient of friction, based on the inclined plane method, consists in placing the balanced rotor on the shaft, Figure 19. An end of the shaft is supported by a fixed body and the other end is slightly raised by supporting it on a cylindrical body. When the body of the rotor starts

sliding, the procedure is stopped and the angle α of tilting of the shaft is found using elementary trigonometry and the coefficient of dynamic friction is thus obtained.

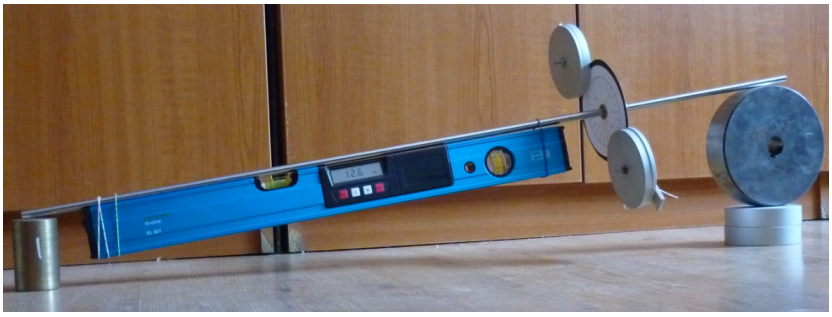

Figure 19. Finding the coefficient of friction $\mu_d = tan(\alpha)$ between the shaft and the bushing.

3.2. Experimental Results

The value of the coefficient of dynamic friction found with the method described above is $\mu_d = 0.167$. Using this value, the curves for the variation of the rotation angle, theoretic and experimental, were traced and are presented in Figure 20. A very good agreement between the theoretical data and the experimental results is observed.

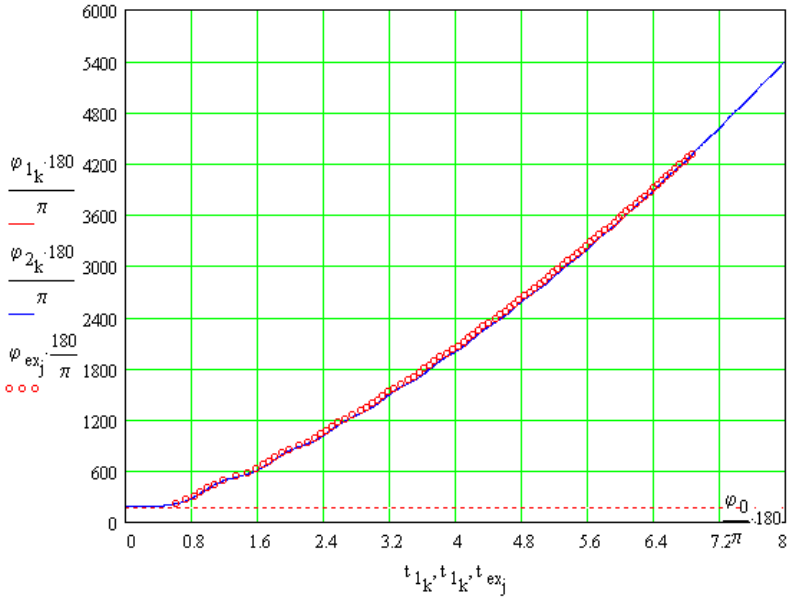

Figure 20. The rotation angle of the rotor: experimental (red circles) and theoretical (blue line for dynamic friction model and red line for static and dynamic friction model).

A better comparison is obtained considering the angular velocity of the model and of the experimental rotor. The dependency $\left(t_{ex_j}, \varphi_{ex_j}\right)$ is numericaly differentiated and the mean value of the angular velocity on the interval $(t_{ex_j} - t_{ex_{j-1}})$ is obtained:

$$\omega_{ex_j} = \frac{\varphi_{ex_j} - \varphi_{ex_{j-1}}}{t_{ex_j} - t_{ex_{j-1}}} \tag{51}$$

The theoretical and experimental angular velocities of the rotor are presented by comparison in Figure 21 and a very good concordance is shown.

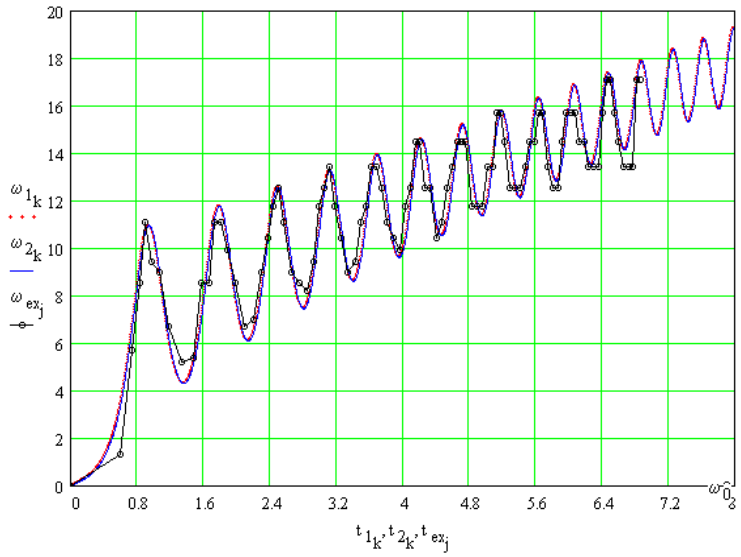

Figure 21. Comparison between theoretical and experimental angular velocities: black points, experimental; blue, theoretical model with dynamic friction and red, theoretical model with static and dynamic friction for $v_{cr} \to 0$.

The attempt to interpolate the experimental data was prevented by the fact that once the transition velocity increases, the only change that occurs is the decrease of the oscillation period of the angular velocity and the rapid increase of its average value. Trying to compensate, even partially, for these effects by a greater coefficient of static friction assumes accepting values which have no correspondence in physical reality ($\mu_{st} = 1.5$) as in Figure 22.

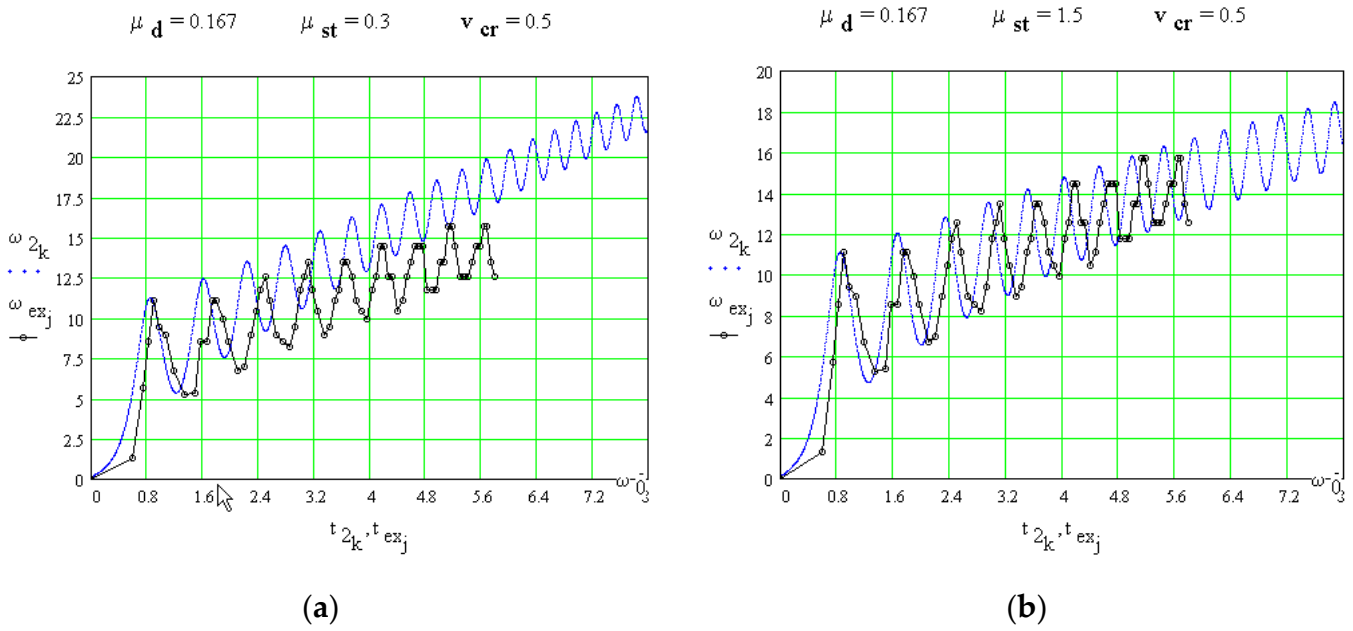

Figure 22. Attempt to interpolate the experimental data considering the second friction model (static-and-dynamic friction): black, experimental and blue, theoretical solution: (**a**) $\mu_d = 0.167$; $\mu_{st} = 0.3$; $v_{cr} = 0.5$ m/s and (**b**) $\mu_d = 0.167$; $\mu_{st} = 1.5$; $v_{cr} = 0.5$ m/s.

In order to validate the hypothesis of rigid rotor, a simulation was accomplished using FEM Catia analysis; it was evidenced that the first proper frequency of the rotor is significantly greater than the working rotational velocities of the experimental rotor. In

Figure 23 screen capture is presented with the first ten proper frequencies and the rotor shape for the fundamental frequency.

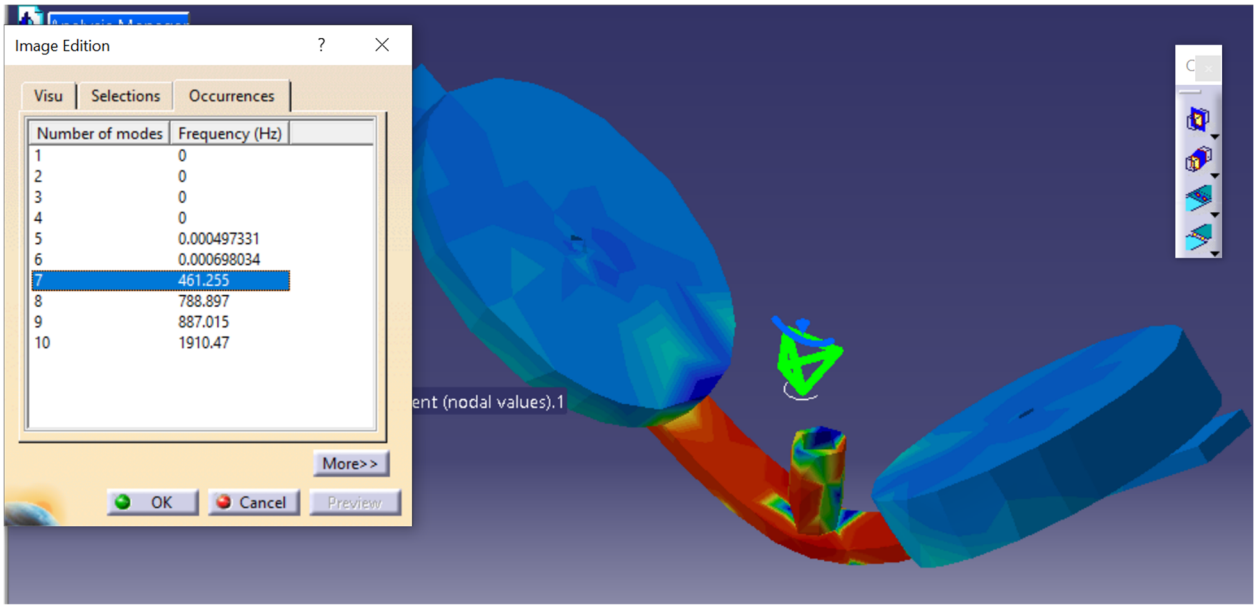

Figure 23. The first ten proper frequencies and the rotor shape for the fundamental frequency.

From these simulations one can remark that the first six values correspond to the displacements of rigid body, and afterwards, that the first fundamental frequency corresponding to bending about an horizontal axis is 461 Hz, while from Figures 22 and 23 it results that the maximum value of the angular velocity is $\omega < 50$ rad/ sec or $n < 10$ sec^{-1}.

The authors propose defining some characteristic parameters for the evolution of the system in the two situations.

For the damped rotor, Figure 24, t_{end} is found to confirm that the signal of the angular velocity is enveloped by the straight line:

$$\omega_e(t) = \alpha t + \beta \tag{52}$$

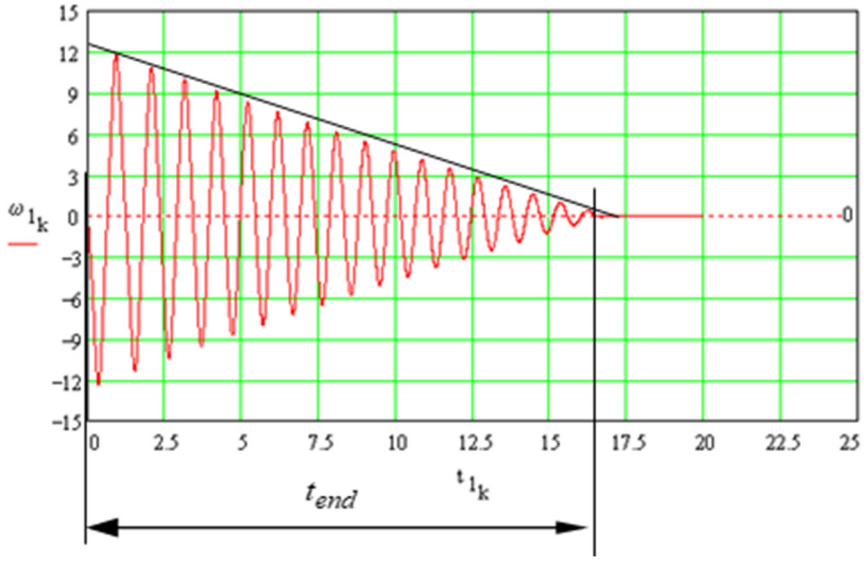

Figure 24. Finding of motion period t_{end} for a damped rotor.

The parameters α and β are found from the condition that the straight line is tangential to the plot of angular velocity, using the least-squares method. The physical significance of these two parameters is obvious: α is the velocity of linear diminishing of the amplitude of angular velocity and β allows for finding the final time of the motion $t_{end} = -\beta/\alpha$.

For the case presented in Figure 25, when the motion of the system becomes permanent, it is proposed that the function that best approximates the mean value of the angular velocity is obtained using the LSM, that is a parabola defined on the interval $[0, t_{ch}]$.

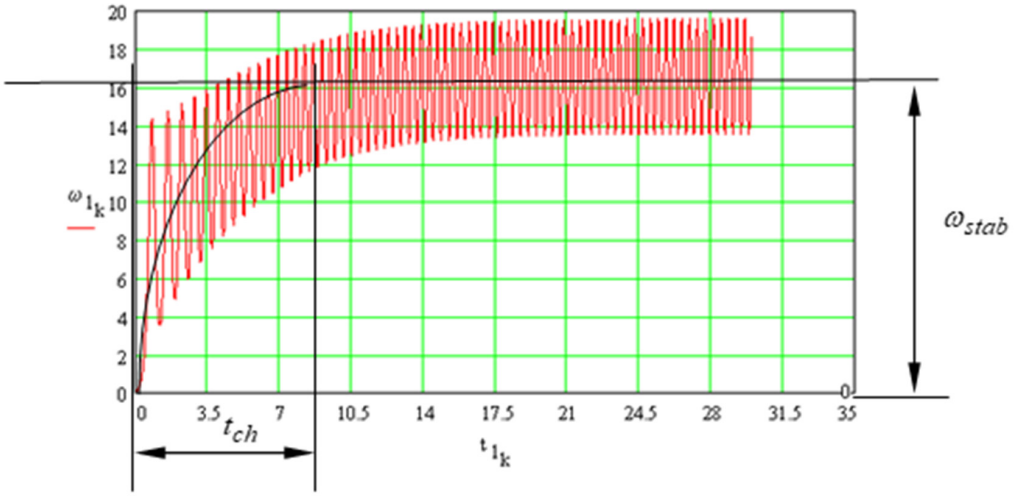

Figure 25. Finding the parameters of t_{ch} and ω_{stab} for a rotor with steady motion.

The t_{ch} value is the time when steady state occurs and ω_{stab} is a value about which the angular velocity varies after the motion becomes permanent,

$$\omega_m(t) = \begin{cases} \alpha\, t^2 + \beta t + \Gamma, if\ t < t_{ch} \\ \omega_{stab}, if\ t > t_{ch} \end{cases} \tag{53}$$

where ω_m is the median line of the angular velocity.

One of the limitations of the model is the small value of the duration times on the actual device, caused by the imposed height at which it is placed in the laboratory. A first change to amend this aspect is using another rotor, with smaller radius R and greater driving mass for obeying the condition $mR = const$, (the same acting torque). Another solution could be the use of an actuating motor with well-stipulated mechanical characteristic; for this situation the calculus must be completed correspondingly.

4. Conclusions

The aim of this paper is the study of the cumulative effect of dry friction and mass eccentricity upon the behaviour of dynamic systems actuated by the gravity force.

The dynamic system consists in a rotor with controlled eccentricity, having a horizontal axis of rotation. The system is set into motion using a mass suspended at the end of an inextensible wire, wound on the shaft of the rotor. It is assumed that dry friction exists in the joint of the rotor. The friction models accepted are two of the simplest existing in the technical literature: the first model, considering Coulomb friction characterised by the coefficient of dynamic friction and the second model, which considers that the friction is characterised with respect to transition velocity: for velocities greater than v_{cr}, the coefficient of static friction is considered and below the critical value, the coefficient varies linearly with the velocity up to a maximum value, equal to the coefficient of static friction.

The equations of the model are obtained for more general conditions, regarding the long rotor supported symmetrically by two coaxial identical bearings with very short length and so, the normal reactions could be assimilated to concentrated forces. Applying the fundamental theorems of dynamics of rigid bodies, the equation of motion of the rotor and

the characteristics of the reaction forces (magnitude and orientation) from the two bearings are obtained. Next, considering that the distance between the two bearings tends to zero, a dynamic model of the short rotor is obtained. The unknowns of the dynamic model of the short rotor are the law of motion and the characteristics of the reaction force (magnitude and orientation) from the bearing.

The model is characterised by the following parameters: tribological characteristics, the values of the coefficients of static friction and dynamic friction, the value of the conventional transition velocity from the static to dynamic regime, the mass of the actuating body, the inertia characteristics of the rotor (mass, position of the centre of mass and axial centric moment of inertia) and the initial conditions (position and angular velocity) together with the parameters of the integration algorithm (time domain and number of divisions).

The most important remark is the fact that the combined effect of dry friction and eccentricity leads to a rotational motion of the rotor either with angular velocity oscillating around a constant value, or damped motion, with angular amplitude decreasing linearly to zero. When there is a lack of dry friction, regardless of the value and type of friction, the angular velocity increases indefinitely. Once the law of motion is established, then the values of the normal reaction, friction force and angular velocity can be found.

In order to decide which of the two laws of friction better describes the behaviour of the model, an experimental device was designed and realised for corroborating the theoretical model. The complex shape of the rotor suggested that is simpler to obtain the values of the dynamic parameters (mass, position of the centre of gravity and moment of inertia with respect to the axis of rotation) by modelling the rotor using CAD software. Another required parameter is the coefficient of friction from the plain bearing. Concerning the static friction, the value of the coefficient was the one recommended by the technical literature.

With the identified shape and dimensions of the rotor, the modelling was possible, using a finite element software which allows for finding the oscillation modes. It is observed that the value of the vibration is considerably higher than the maximum rotation velocity reached by the rotor during the experimental tests.

In order to validate the proposed theoretical model, the law of motion of the experimental rotor was found. For minimum disturbance upon the evolution of the dynamic system, the rotor was filmed with a high-speed video-recording camera and afterwards, the movie was split into frames, using software, to determine the numerical dependency of the angle of rotation with respect to time.

The experimental data were numerically differentiated, and the experimental variation of the angular velocity of the rotor was obtained. The plots of experimental variation of the angle and angular velocity of the rotor were compared to the theoretical variations for the two friction models considered and it was concluded that the model considering only dynamic friction interpolates the experimental data in an excellent manner. The attempt to apply the model with static friction for significant values of the transition velocity proved inadequate because an acceptable interpolation is obtained only for unrealistic tribological parameters.

One of the limitations of the experimental set up resides in the relatively short actuating time of the driving mass, due to the small value of the positioning height (on vertical direction) of the device. In order to improve this aspect, the employment of a greater driving mass and diminished diameter of the winding shaft of the wire is proposed.

The paper can be continued with other research concerning mainly the application of more complex dry friction models [40], as well as the fluid friction rotor; another direction can consider different types of actuation (spring, direct current etc.).

An alternative generalization of the model consists in actuating with a driving motor with well-stipulated characteristics, capable of activating the rotor with rotation velocities comparable to the resonant frequencies, in order to highlight the differences between the rotor assumed rigid and the rotor supposed to be a deformable body.

Author Contributions: Conceptualization, S.A. and I.M.; methodology, C.B. and S.A.; software I.-C.R., N.-A.N. and S.A.; validation, N.-A.N., I.-C.R. and F.-C.C.; writing—original draft preparation, S.A. and F.-C.C.; writing—review and editing, C.B. and F.-C.C. and supervision, I.M. and S.A.; All authors have read and agreed to the published version of the manuscript.

Funding: This research received no external funding.

Conflicts of Interest: The authors declare no conflict of interest.

References

1. Davidson, J.K.; Hunt, K.H. *Robots and Screw Theory: Applications of Kinematics and Statics to Robotics*, 1st ed.; Oxford University Press: New York, NY, USA, 2004; pp. 134–191.
2. Spurr, R.T. A theory of brake squeal. *Proc. Auto. Div. Instn. Mech. Engrs.* **1961**, *1*, 33–40. [CrossRef]
3. Nelson, H. Rotordynamics modeling and analysis procedures: A review. *JSME Intern. J. Ser. C* **1998**, *41*, 1–12.
4. Kirk, R.G.; Gunter, E.J. Short bearing analysis applied to rotor dynamics Part 1: Theory. *J. Lubr. Technol.* **1976**, *169*, 47–56. [CrossRef]
5. Kirk, R.G.; Gunter, E.J. Short bearing analysis applied to rotor dynamics Part 2: Results of journal bearing response. *J. Lubr. Technol.* **1976**, *169*, 159–169. [CrossRef]
6. Kumar, A.; Kumar, P. An application of short bearing theory to analyses the effect of variable permeability on steady performance of turbulent hydrodynamic porous journal bearings. *Indian J. Eng. Mater. Sci.* **1996**, *1*, 57–62.
7. Kascak, A.F. *Direct Integration of Transient Rotor Dynamics*; Technical report; Lewis Research Center: Cleveland, OH, USA, 1980.
8. Fu, C.; Sinou, J.J.; Zhu, W.; Lu, K.; Yang, Y. A state-of-the-art review on uncertainty analysis of rotor systems. *Mech. Syst. Signal Process* **2023**, *183*, 1–41. [CrossRef]
9. Rendl, J.; Byrtus, M.; Dyk, S.; Smolik, L. Subcritical behaviour of short cylindrical journal bearings under periodic excitation. *Nonlinear Dyn.* **2023**, *111*, 1–14. [CrossRef]
10. Lin, C.G.; Yang, Y.N.; Chu, J.L.; Sima, C.; Liu, P.; Qi, L.B.; Zou, M.S. Study on nonlinear dynamic characteristics of propulsion shafting under friction contact of stern bearings. *Tribol. Int.* **2023**, *183*, 1–13. [CrossRef]
11. Paulo, P. A Time-Domain Methodology for Rotor Dynamics: Analysis and Force Identification. Master's Thesis, Technical University of Lisbon, Lisbon, Portugal, 2011.
12. Wagner, M.B.; Younan, A.; Allaire, P.; Cogill, R. Model reduction methods for rotor dynamic analysis: A survey and review. *Int. J. Rotating Mach.* **2011**, *2010*, 273716. [CrossRef]
13. Kinkaid, N.M.; O'Reilly, O.M.; Papadopoulos, P. Review automotive disc brake squeal. *J. Sound. Vib.* **2003**, *267*, 105–166. [CrossRef]
14. Pavlović, R.; Kozić, P.; Janevski, G. Influence of rotatory inertia on stochastic stability of a viscoelastic rotating shaft. *Theoret. Appl. Mech.* **2008**, *35*, 363–379. [CrossRef]
15. Genta, G. Introduction. In *Dynamics of Rotating Systems*, 2005th ed.; Genta, G., Ed.; Springer: New York, NY, USA, 2005; Volume 1, pp. 1–31.
16. Genta, G. Dynamic behavior of free rotors. In *Dynamics of Rotating Systems*, 2005th ed.; Genta, G., Ed.; Springer: New York, NY, USA, 2005; Volume 1, pp. 413–463.
17. Choi, Y.S.; Noah, S.T. Nonlinear steady-state response of a rotor-support system. *J. Vib. Acoust.* **1987**, *109*, 255–261. [CrossRef]
18. Zheng, W.; Aghababaei, R.; Hong, J.; Pei, S. An efficient method for transient response of rotor systems based on squeeze film damper. *Tribol. Int.* **2023**, *183*, 1–10. [CrossRef]
19. Liu, N.Y.; Ouyang, H.J. Friction-induced vibration of a slider on an elastic disc spinning at variable speeds. *Nonlinear Dyn.* **2019**, *98*, 39–60. [CrossRef]
20. Yang, L.; Zhang, J.; Guo, Y. Uncertainty representation and quantification for a nonlinear rotor/stator system with mixed uncertainties. *J. Vibroeng.* **2016**, *18*, 4836–4851. [CrossRef]
21. Marino, L.; Cicirello, A. Experimental investigation of a single-degree-of-freedom system with Coulomb friction. *Nonlinear Dyn.* **2020**, *99*, 1781–1799. [CrossRef]
22. Adiletta, G.; Guido, A.R.; Rossi, C. Nonlinear dynamics of a rigid unbalanced rotor in journal bearings. Part I: Theoretical analysis. *Nonlinear Dyn.* **1997**, *14*, 57–87. [CrossRef]
23. Adiletta, G.; Guido, A.R.; Rossi, C. Nonlinear dynamics of a rigid unbalanced rotor in journal bearings. Part II: Experimental analysis. *Nonlinear Dyn.* **1997**, *14*, 157–189. [CrossRef]
24. Matsushita, O.; Tanaka, M.; Kobayashi, M.; Keogh, P.; Kanki, H. *Vibrations of Rotating Machinery. Volume 1. Basic Rotordynamics: Introduction to Practical Vibration Analysis*, 1st ed.; Springer: Tokyo, Japan, 2017; pp. 41–78.
25. Matsushita, O.; Tanaka, M.; Kobayashi, M.; Keogh, P.; Kanki, H. *Vibrations of Rotating Machinery. Volume 2. Advanced Rotodynamics: Applications of Analysis, Troubleshooting and Diagnosis*, 1st ed.; Springer: Tokyo, Japan, 2020; pp. 19–40.
26. Wagner, N.; Helfrich, R. Dynamics of rotors in complex structures. In Proceedings of the NAFEMS World Congress, Salzburg, Austria, 9–12 June 2013.
27. Creci, G.; Menezes, J.C.; Barbosa, J.R.; Corra, J.A. Rotordynamic analysis of a 5-kilonewton thrust gas turbine by considering bearing dynamics. *J. Propuls. Power* **2011**, *27*, 330–336. [CrossRef]

28. Shaw, J.; Shaw, S.W. Instabilities and bifurcations in a rotating shaft. *J. Sound. Vib.* **1989**, *132*, 227–244. [CrossRef]
29. Badgley, R.H.; Booker, J.F. Rigid-body rotor dynamics: Dynamic unbalance and lubricant temperature changes. *ASME J. Lubr. Technol.* **1970**, *92*, 415–421. [CrossRef]
30. Rao, J.S. *Rotor Dynamics*, 1st ed.; John Wiley & Sons: Hoboken, NJ, USA, 1983; pp. 73–84.
31. Dimarogonas, A.D.; Paipetis, S.A.; Chondros, T.G. Mathematical Models for Rotor Dynamic Analysis. In *Analytical Methods in Rotor Dynamics*, 2nd ed.; Dimarogonas, A.D., Paipetis, S.A., Chondros, T.G., Eds.; Springer: Dordrecht, The Netherlands, 2013; Volume 9, pp. 43–75.
32. Subbiah, R.; Littleton, J. Mathematical model. In *Rotor and Structural Dynamics of Turbomachinery: A Practical Guide for Engineers and Scientists*, 1st ed.; Subbiah, R., Littleton, J., Eds.; Springer: New York, NY, USA, 2018; Volume 1, pp. 25–72.
33. Sinou, J.J.; Nechak, L.; Besset, S. Kriging Metamodeling in Rotordynamics: Application for Predicting Critical Speeds and Vibrations of a Flexible Rotor. *Complexity* **2018**, *2018*, 1264619. [CrossRef]
34. Armanini, C.; Dal Corso, F.; Misseroni, D.; Bigoni, D. Configurational forces and nonlinear structural dynamics. *J. Mech. Phys. Solids* **2019**, *130*, 82–100. [CrossRef]
35. Li, Z.M.; Liu, T.; Kang, H.; Tian, J.; Jing, J.; Wang, D. Theoretical and experimental investigations on steady-state responses of rotor-blade systems with varying rotating speeds based on a new nonlinear dynamic model. *Mech. Syst. Signal Process.* **2023**, *184*, 109692. [CrossRef]
36. Tang, P.; Zehnder, J.; Coros, S.; Thomaszewski, B. A harmonic balance approach for designing compliant mechanical systems with nonlinear periodic motions. *ACM T Graph.* **2020**, *39*, 1–14. [CrossRef]
37. Liu, G.; Chen, G.; Cui, F.; Xi, A. Nonlinear vibration analysis of composite blade with variable rotating speed using Chebyshev polynomials. *Eur. J. Mech. A Solids* **2020**, *82*, 103976. [CrossRef]
38. Shi, X.; Chatzis, M.N. Lie symmetries of nonlinear systems with unknown inputs. *Mech. Syst. Signal. Process.* **2023**, *188*, 110027. [CrossRef]
39. Vetyukov, Y.; Oborin, E. Snap-through instability during transmission of rotation by a flexible shaft with initial curvature. *Int. J. Non Linear Mech.* **2023**, *154*, 104431. [CrossRef]
40. Flores, P.; Lankarani, H.M. *Contact Force Models for Multibody Dynamics*; Solid Mechanics and Its Applications Series; Springer International Publishing: Cham, Switzerland, 2016; Volume 226, p. 171.
41. Marques, F.; Flores, P.; Claro, I.C.P.; Lankarani, H.M. A survey and comparison of several friction force models for dynamic analysis of multibody mechanical systems. *Nonlinear Dyn.* **2016**, *86*, 1407–1443. [CrossRef]
42. Ardema, M.D. Review of newtonian dynamics. In *Analytical Dynamics: Theory and Applications*, 2005th ed.; Ardema, M.D., Ed.; Springer: New York, NY, USA, 2004; Volume 1, pp. 1–45.
43. Pavlenko, I.; Verbovyi, A.; Neamţu, C.; Ivanov, V.; Ciszak, O.; Trojanowska, I. Fractional-order mathematical model of single-mass rotor dynamics and stability. *Alex. Eng. J.* **2023**, *76*, 91–100. [CrossRef]
44. Koshy, C.S.; Flores, P.; Lankarani, H.M. Study of the effect of contact force model on the dynamic response of mechanical systems with dry clearance joints: Computational and experimental approaches. *Nonlinear Dyn.* **2013**, *73*, 325–338. [CrossRef]
45. Alaci, S.; Kalitchin, Z.; Kandeva, M.; Ciornei, F.C.; Bujoreanu, C.; Machado, J. Simple technique and device for slurries viscosity measurement. *J. Environ. Prot. Ecol.* **2019**, *20*, 761–772.
46. Chen, G.S.; Liu, X. *Friction Dynamics-Principles and Applications*, 1st ed.; Woodhead Publishing: Cambridge, UK, 2016; pp. 247–298.